Spatial-temporal changes in flow hydraulic characteristics and soil loss during gully headcut erosion

Mingming Guo[a], Zhuoxin Chen[b], Wenlong Wang[b,c*], Tianchao Wang[d], Qianhua Shi[b], Hongliang Kang[b], Man Zhao[b], Lanqian Feng[c]

a Key laboratory of Mollisols Agroecology, Northeast Institute of Geography and Agroecology, Chinese Academy of Sciences, Harbin 150081, Heilongjiang, China

b State Key Laboratory of Soil Erosion and Dryland Farming on the Loess Plateau, Institute of Water and Soil Conservation, Northwest A&F University, Yangling, Shaanxi 712100, China

c Institute of Soil and Water Conservation, Chinese Academy of Sciences and Ministry of Water Resources, Yangling, Shaanxi 712100, China

d Ulanyab Grassland Station, Jining, Inner Mongolia 012000, China

***Corresponding author:** Wenlong Wang

E-mail addresses: nwafu_wwl@163.com; wlwang@nwsuaf.edu.cn

Abstract

The temporal-spatial changes in flow hydraulics and energy consumption and their associated soil erosion remain unclear during gully headcut retreat. A simulated scouring experiment was conducted on five headcut plots consisting of upstream area (UA), gully headwall (GH) and gully bed (GB) to elucidate the temporal-spatial changes in flow hydraulic, energy consumption, and soil loss during headcut erosion. The flow velocity at the brink of headcut increased as a power function of time, whereas the jet velocity entry to plunge pool and jet shear stress logarithmically or linearly decreased over time. The jet properties significantly affected by upstream flow. The Reynold number, runoff shear stress, and stream power of UA and GB increased as logarithmic or power functions of time, but the Froude number decreased logarithmically over time. The flow of UA and GB was supercritical and subcritical, respectively, and transformed to turbulent with inflow discharge increased. The Reynold number, shear stress and stream power decreased by 56.0%, 63.8% and 55.9%, respectively, but the Froude number increased by 7.9% when flow dropped from UA to GB. The accumulated runoff energy consumption of UA, GH and GB positions linearly increased with time, and their proportion of energy consumption are 18.3%, 77.7% and 4.0%, respectively. The soil loss rate of the "UA-GH-GB" system initially rose and then gradually declined and levelled off. The soil loss of UA and GH decreased logarithmically over time, whereas the GB was mainly characterized by sediment deposition. The proportion of soil loss at UA and GH are 11.5% and 88.5%, respectively, of which the proportion of deposited sediment on GB reached 3.8%. The change in soil loss of UA, GH and GB was significantly affected by flow hydraulic and jet properties. The critical energy consumption initiating soil erosion of UA, GH, and GB are 1.62 J s^{-1}, 5.79 J s^{-1} and 1.64 J s^{-1}, respectively. These results are helpful to reveal the mechanism of gully headcut erosion and built headcut migration model.

Keywords: Gully erosion; Hydraulic property; Headcut retreat; Bank collapse; Loess Plateau

1 Introduction

Gully erosion is a typical soil erosion process whereby concentrated runoff from a upstream drainage area recurs in a channel and erodes soil from the area through which runoff passed to considerable depth (Poesen et al., 2003; Zhu, 2012). Gully erosion is recognized as the main sediment source in some hilly and gully-dominated watersheds (Poesen et al., 2003; Valentin et al., 2005; Dotterweich et al., 2012). Poesen et al. (2003) reported that soil loss amount caused by gully erosion accounts for 10% - 94% of total soil loss amount based on the collected data from published articles. Moreover, gully erosion can severely damage to infrastructure, enhance the terrain fragmentation, and cause ecosystem instability, land degradation and food safety (Poesen et al., 2003; de Vente & Poesen, 2005; Li et al., 2015; Vanmaercke et al, 2016; Hosseinalizadeh et al., 2019).

As one of the gully erosion processes, the gully headcut retreat often significantly influences and determines gully erosion (Oostwoud-Wijdenes et al., 2000; Vandekerckhove et al., 2003; Guo et al., 2019). A headcut is defined as a vertical or near-vertical drop or discontinuity on the bed of a gully occurring where flow is concentrated at a knickpoint (Hanson et al., 2001; Bennett et al., 2000). Many studies have demonstrated that the gully erosion is the result of the combined actions of plunge pool erosion by jet flow, upstream runoff incision, headwall erosion by on-wall flow, mass failure (gully head and wall collapse), (Vanmaercke et al., 2016; Addisie et al., 2017; Guo et al., 2019). Once a headcut is formed in upstream area, the gully will develop rapidly and not stop forward until a critical topographic condition is formed ($S \leq a \cdot A^b$, where S and A is the slope gradient and drainage area upstream gully headcut, respectively) (Kirkby et al., 2003). Moreover, in fact, the erosion processes of different landform units (upstream area, UA; gully head, GH; gully bed, GB) are completely different during gully headcut erosion (Zhang et al., 2018; Guo et al., 2019; Shi et al., 2020a). The combination and interaction of erosion processes of the three landform units determined gully headcut erosion process (Vanmaercke et al., 2016). Therefore, clarifying the soil erosion process and characteristics of the three landform units is critical to systematically and clearly reveal the mechanism of gully headcut erosion.

Previous studies suggested that gully heacut erosion is affected by various factors including topography, land use change, vegetation, soil properties, and climate (Vanwalleghem et al., 2003;

Ionita, 2006; Rodzik et al., 2009; Rieke-Zapp and Nichols, 2011; Torri and Poesen, 2014; Ionita et al., 2015; Vannoppen et al., 2015; Guo et al., 2019, 2020a). In terms of topography, most of studies focused on the threshold relationship ($S \leq a \cdot A^b$) to initiate gully erosion (e.g. Torri and Poesen, 2014). Several experimental studies demonstrated that the upstream slope gradient and headcut height have significant effects on headcut erosion (e.g. Bennett, 1999; Zhang et al., 2018). Land use change is recognized as having the strongest effect on processes related to gully erosion among influencing factors (Poesen et al., 2003; Chaplot et al., 2005; Descroix et al., 2008), and also significantly affects the activation of gully headcut erosion (e.g. Torri and Poesen, 2014). In this aspect, the vegetation coverage is a parameter that is often used to clarify its effect on gully erosion (e.g. De Baets et al., 2007; Martínez-Casasnovas et al., 2009), however, in fact, the vegetation effect mainly depended on the root characteristics and its distribution at gully head (e.g. Vannoppen et al., 2015; Guo et al., 2019). Nevertheless, at present, the most of studies on gully erosion focus on the changes in gully morphology between different periods at a watershed or regional scale (Vanmaercke et al., 2016), which is why the previous studies fail to address the effects of root systems on gully headcut retreat. Guo et al. (2019) concluded that the grass (*Agropyron cristatum*) could reduce soil loss and headcut retreat distance by 45.6–68.5%, 66.9–85.4%, respectively, and the roots of 0–0.5 mm in diameter showed the greatest controlling influence on headcut erosion. In terms of soil properties, lots of studies have proved the significant effect of soil properties on gully headcut erosion (e.g. Nazari Samani et al., 2010), which was mainly related to the change in soil erodibility induced by soil properties including soil texture, soil vertical joints, soluble mineral content, soil lithology, and physicochemical properties (Sanchis et al., 2008; Vanmaercke et al., 2016; Guo et al., 2020a). Rainfall, the main climate factor, is closely related to runoff generation and thus be expected to affect headcut erosion. Many studies have reported that the initiation of gully headcut is correlated with rainfall characteristics (e.g. summation of rainfall from 24-hour rains equal to or greater than 0.5 inches) (Beer and Johnson, 1963; Vandekerckhove et al., 2003; Rieke-Zapp and Nichols, 2011). However, the great difference in the threshold value relating to rainfall factors was found among different areas of the world due to great difference in erosion environment. For example, in the northeast of China, the gully erosion is the result of soil thawing, rainfall runoff and snowmelt runoff

(Li et al., 2016b; Xu et al., 2019). Furthermore, at present, the most of studies on gully erosion were conducted to quantify the change in gully erosion (retreat rate, area and volume) at different spatial and temporal scales by using remote sensing interpretation, real-time monitoring and meta-analysis based on literature data (e.g. Vanmaercke et al., 2016). However, the influencing mechanism of these factors on gully headcut erosion is still unclear and need to be revealed in future studies.

Evidently, the concentrated flow upstream gully head, mainly depended on the upstream area and rainfall, is the main and original drive force triggering headcut erosion. The runoff firstly eroded the upstream area and then was parted into two types of flow (on-wall flow and jet flow) at the brinkpoint of gully headcut. Consequently, the on-wall flow persistently eroded the headwall soil, and the jet flow violently impacted gully bed soil and formed a plunge pool (Su et al., 2015; Guo et al., 2019). Subsequently, the two types of flow merged again and eroded gully bed together (Zhang et al., 2018; Shi et al., 2020a). The runoff hydraulic or jet flow properties at different landform units (upstream area, gully head and gully bed) are significantly different, which is an important reason for the difference in erosion process among different landform units. However, the temporal-spatial change in runoff and jet properties during headcut erosion is still unclear and thus needs to be clarified. Furthermore, at present, some experimental studies on headcut erosion of rill, ephemeral gully, gully and bank gully were conducted to investigate the runoff properties, energy consumption, sediment transport process, morphology evolution and empirical model (Bennett and Casalí, 2001; Wells et al., 2009a, 2009b; Su et al., 2014; Xu et al., 2017a; Guo et al., 2019; Shi et al., 2020a). However, relatively few knowledges were obtained to systemically reveal the hydrodynamic mechanism of gully headcut erosion. Therefore, elucidating the temporal-spatial changes in runoff hydraulic and soil loss and hydrodynamic mechanism of UA, GH and GB is of great importance to systematically reveal the hydrodynamics mechanism of gully headcut erosion.

Given the above-mentioned issues, a series of simulated gully headcut erosion experiments subjected to inflow scouring are conducted to (1) investigate the temporal-spatial change in hydraulic properties and soil loss during headcut erosion, (2) quantify the energy consumption and soil loss distribution of UA, GH and GB, and (3) reveal the erosion hydrodynamic mechanism of UA, GH and GB.

2 Materials and Methods

2.1 Study area

This experiment was carried out at the Xifeng Soil and Water Conservation Experimental Station that is located in the Nanxiaohegou watershed, Qingyang City, Gansu Province, China (Fig. 1). The study area belongs to a semi-arid continental climate with a mean annual temperature of 9.3 °C. The mean annual precipitation is 546.8 mm (1954 - 2014), of which precipitation from May to September accounts for 76.9% of the total precipitation. The elevation ranges from 1050 to 1423 m (Xia et al., 2017; Guo et al., 2019). The main landforms include gentle loess-tableland, steep hillslope and gully channel, and their areas account for 57.0%, 15.7% and 27.3%, respectively. The loess-tableland is characterized by low slope (1–5°), gentle and flat terrain and fertile soil. The main soil type is loessial soil with silt loam texture. Most of hillslopes have been constructed as slope-terraces. The main gully channel is usually U-shaped and the branch-gully is more actively developed and easily eroded as a V-shaped by runoff from loess-tableland (Xu et al., 2019). The flat loess-tableland can accumulate the 67.4% of total runoff and cause serious gully erosion that can contribute 86.3% of the total soil erosion (Guo et al., 2019). The original plant species have been seriously destroyed. Since the 1970s, the "Three Protection Belts" system, the "Four Eco-Economical Belts" system and the "Grain for Green" project (Zhao, 1994; Fu et al., 2011) were implemented to control soil erosion. The current mean annual soil erosion rate has been reduced to 4350 t km^{-2} y^{-1} in the study watershed (Guo et al., 2019). The previous vegetation are mainly artificially planted forests and some native secondary herbaceous communities.

2.2 Experimental design

2.2.1 Gully head experimental plot construction

Five gully head plots for headcut erosion experiments were constructed at the experimental station in April 2018. Fig. 2 shows the basic information of the gully head plot consisting of three landform units (upstream area, headwall and gully bed). The plot width and slope gradient of upstream area and gully bed are uniformly designed as 1.5 m and 3°, respectively. The upstream area length, the height of the vertical headwall and the length of the gully bed are 5.0 m long, 0.9 m, and

1.0 m, respectively (Fig. 2a). The plot boundary was constructed in strict accordance with designed plot dimension using cement and bricks (Fig. 2b). After the construction of plot boundary, the soil was sieved through a 2 cm sieve with to remove roots and debris and ensure uniform soil underlying condition. The sieved soil was filled into the plot every 10-cm thick layer according to the investigated soil bulk density of gully heads. The soil surface of each layer was harrowed to increase the cohesion between two soil layers (Guo et al., 2019). In general, the filling upstream area length was 5.5 m that was larger than the precise upstream area length (5.0 m). After establishment of gully head plots, the five plots were carefully managed about four months (August 2018) to allow the soil to return to its natural state. During the four-month conservation process, the naturally growing weeds were weeded out in time. Moreover, a flow-steady tank of 0.6 m, 1.5 m and 0.5 m in length, width and height was installed at the top of upstream area, and a circular sampling pool of 0.6 m in diameter was set at the bottom of the gully bed to collect runoff and sediment (Fig. 2a).

2.2.2 Inflow discharge design

The concentrated runoff generated from upstream area is the main force driving gully headcut erosion. Jiao et al (1999) concluded that the more serious soil erosion is generally caused by "A" type rainstorm with the rainfall duration of 25 to 178 mins than other types of rainstorms in the Loess Plateau. Thus, an extreme case of rainfall duration (180 min) was considered in this study, and the recurrence period of "A" type rainstorm was designed as 30 years. Previous studies indicated that the rainstorm distribution on the Loess Plateau showed a non-significant change in past decades (Li et al., 2010; Sun et al., 2016; Wen et al., 2017). Zhang et al. (1983) proposed a statistical equation (Eq. (1)) for calculating the average rainfall intensity by analyzing 1710 typical rainstorm events in the Loess Plateau. Then, the inflow discharge was calculated by Eq. (2) and ranged from 3.12 to 9.68 m^3 h^{-1}. Considering the pre-experiment effect, finally, we selected the five inflow discharge levels (3.0, 3.6, 4.8, 6.0, and 7.2 m^3 h^{-1}).

$$RI = \frac{5.09N^{0.379}}{(t+1.4)^{0.74}} \quad (1)$$

where RI is the average rainfall intensity during t minutes, mm min^{-1}; N is the recurrence period of rainstorm, yr; and t is the rainfall duration, min.

$$q = \frac{60\alpha \cdot A \cdot RI \cdot w}{W} \quad (2)$$

where A is the upstream area (km^2) and has a wide range of 0.15 - 8.7 km^2 according to an early investigation of research team (Che, 2012); W is the width of the upstream area, km; w is the plot width, m; and α is the runoff coefficient of bare land and is identified as 0.167 by analyzing the runoff and rainfall data of standard runoff plots (Li et al., 2006).

2.3 Experimental procedure

The scouring experiment was conducted in August 2018. Before formal experiment, firstly, the upstream area length was adjusted to designed length of 5.0 m (Fig. 3a). Then, a self-made tent (length × width × height: 6.0 m × 3.0 m × 3.5 m) with waterproof canvas enclosed the plot to resist the effect of natural rainfall and sunshine on experimental progress and photo shooting for 3D reconstruction (Fig. 2b). In addition, the experimental process was recorded by two Logitech 930e video cameras with a resolution of 2.0 megapixels. The camera 1 was installed 2.5 m in front of plot headwall (Fig. 2a), and the camera 2 was installed 3.0 m above the plot center (Fig. 2a).

Before the experiment, watering can be used to spray each experimental plot until surface runoff was generated, and then the plot was placed for 24 hours to ensure adequate water infiltration, which can assure that the soil moisture of the five plots was approximately the same. The inlet pipeline was placed in steady flow tank when the inflow discharge was adjusted to designed value. A water thermometer was placed into the steady flow tank to monitor the change in water temperature during experimental process. The runoff and sediment samples at the plot outlet were collected at 2-min intervals to represent the temporal change in runoff and sediment of "UA – GH – GB" system, and the sampling time was also recorded using a stopwatch (Fig. 3b). The runoff and sediment samples were oven-dried at 105 °C for 24 h and weighed to calculate the soil loss rate of the "UA – GH – GB" system ($g\ s^{-1}$). Besides, the timing of the collapse events were also recorded during headcut erosion. The upstream area was divided into 4 runoff observation sections, and the runoff width (w), depth (d) and velocity (V) of each section were measured by a calibrated scale of 1 mm accuracy and color tracer method (Fig. 3b, 3c). The runoff velocity (V_J) before runoff arrived at the brink of headcut was measured 5 – 8 times by the velocity measuring instrument (LS300-A) with the accuracy of 0.01 m s^{-1}, and the runoff width at the headcut brinkpoint was measured (Fig. 3d). The runoff width and

velocity of gully bed were also measured using the same method with upstream area (Fig. 3e). Above mentioned measurements of runoff characteristics and sediment samples were finished in 2-min intervals. The whole experimental process was recorded by two video cameras and imported into computers (Fig. 3f). In addition to above runoff parameters, the runoff depth (d_b) at the brink of headcut, the plunge pool depth (D_H) and the vertical distance (h) from brink-point of headcut to water surface of plunge pool were also measured 3 - 5 times by a steel ruler with 1 mm accuracy within each 2-min intervals (Fig. 4).

To obtain the temporal change in morphological characteristics during gully headcut erosion, the experimental duration (180 min) was divided into six stage (30 – 60 – 90 – 120 – 150 – 180 min). Photo-based three-dimensional (3D) reconstruction method was employed to obtain the digital elevation model data of each plot prior to experiment and after each 30-min test. 14 target points were placed around the plot for identifying the 3D coordinate before the photos were taken. The eroded photographic was recorded by a Nikon D5300 camera with the focal length of 50 mm. The following aspects were required during photos shooting: (1) obvious water on soil surface and direct sunshine should be avoided, (2) a minimum overlap of 60% between subsequent photographs was required, and (3) some complex eroded photographic should be taken in detail. In this study, the upper left corner of the plot was set as the original coordinates (0, 0, 0) , and the direction of three-dimensional coordinate was determined as shown in Fig. 3d. These collected photos were imported in Agisoft PhotoScan software (Agisoft LLC, Russia, professional version 1.1.6), and then these control points and their coordinates would be identified and entered. The root mean square errors of the target points are 0.0037, 0.0045, 0.0024, 0.0052 and 0.0030 m on average, respectively, for the experiments of five inflow discharges, which can satisfy the study requirement (millimeter level). The DEM could be exported and was used to extract the morphological parameters and soil loss volume of three landform units at six stages (Frankl et al., 2015).

2.4 Parameter calculation, data analysis and figure plotting

2.4.1 Hydraulic parameters of upstream area and gully bed

Five parameters including runoff velocity (V, m s^{-1}), Reynold number (Re), Froude number (Fr),

shear stress (τ, Pa) and stream power (ω, W m^{-2}) were used to characterize the changes in hydraulic properties at upstream area and gully bed positions. The five parameters are calculated as follows.

$$\mathrm{Re} = \frac{V \cdot R}{\upsilon} \quad (1)$$

$$\mathrm{Fr} = \frac{V}{\sqrt{g \cdot R}} \quad (2)$$

$$R = \frac{w \cdot d}{w+2d}, \upsilon = \frac{1.775\times10^{-6}}{1+0.0337T+0.000221T^2} \quad (3)$$

$$\tau = \rho_w \cdot g \cdot R \cdot J \quad (4)$$

$$\omega = \tau \cdot V \quad (5)$$

where R (m) and υ (m^2 s^{-1}) are the hydraulic radius and the water kinematic viscosity coefficient, respectively; w (m), d (m) and T (℃) are the runoff width, depth and water temperature, respectively; ρ_w (kg m^{-3}) is the water density and J (m m^{-1}) is the hydraulic gradient.

2.4.2 Jet properties of gully head

Based on the measured runoff velocity (V_J, m s^{-1}) before runoff arrived at the headcut brinkpoint, the runoff depth (d_b, m) at the headcut brinkpoint, the plunge pool depth (D_H, m) and the vertical distance (h, m) (Fig. 4a), the three parameters including the runoff velocity at the headcut brinkpoint (V_b), jet-flow velocity entry to plunge pool (V_e) and jet-flow shear stress (τ_j) were calculated to clarify the change of jet properties (Rouse, 1950; Hager, 1983; Stein et al., 1993; Flores-Cervantes et al., 2006; Zhang et al., 2016). The three parameters were calculated as follows.

$$V_b = \begin{cases} \frac{\sqrt[3]{q \cdot g}}{0.715}, Fr < 1 \\ V_J \cdot \frac{Fr^2+0.4}{Fr^2}, Fr > 1 \end{cases} \quad (5)$$

$$Fr = \frac{V_J}{\sqrt{g \cdot d_b}} \quad (6)$$

$$V_e = \frac{V_b}{cos\theta_e}, \theta_e = \arctan\left(\frac{\sqrt{2g \cdot D_H}}{V_b}\right) \quad (7)$$

$$\tau_j = 0.025\left(\upsilon/q\right)^{0.2} \cdot \rho_w \cdot \left[2g \cdot (h + d_b/2) + V_b^2\right] \quad (8)$$

2.4.3 Energy consumption of upstream area, gully head and gully bed

In this study, energy consumption of three landform units (upstream area, UA; gully head, GH;

gully bed, GB) were calculated according to the measured runoff characteristic parameters. The bottom of GB was treated as the zero potential surface to quantify the energy consumption. Therefore, the total runoff energy (E_T, J s^{-1}), the runoff energy at the brink of headcut (E_L, J s^{-1}), the runoff energy when runoff leaves the plunge pool (E_H, J s^{-1}), and the runoff energy at the bottom of gully bed (E_B, J s^{-1}) were calculated as following.

$$E_T = \rho_w g q\left[\left(L_l + L_g\right)tan\theta + H_h\right] \quad (9)$$

$$E_L = \rho_w g q\left[\left(L_m + L_g\right)tan\theta + H_h\right] + \frac{1}{2}\rho_w q V_J^2 \quad (10)$$

$$E_H = \rho_w g q\left(L_m + L_g - V_b\sqrt{\frac{2h}{g}}\right)tan\theta + \frac{1}{2}\rho_w q V_P^2 \quad (11)$$

$$E_B = \frac{1}{2}\rho_w q V_B^2 \quad (12)$$

where the L_l (m) and L_g (m) are the projection length of UA and GB, respectively, during gully head migration; L_m (m) is the gully head retreat distance; H_h (m) is the initial gully headcut height. V_P (m s^{-1}) and V_B (m s^{-1}) are the runoff velocity runoff leaving the plunge pool and GB, respectively.

Therefore, the total runoff energy consumption (ΔE_T, J s^{-1}), the runoff energy consumption of UA (ΔE_L, J s^{-1}), the runoff energy consumption of GH (ΔE_H, J s^{-1}) and the runoff energy consumption of GB (ΔE_B, J s^{-1}) could be calculated as follows.

$$\Delta E_T = E_T - E_B \quad (13)$$

$$\Delta E_L = E_T - E_L \quad (14)$$

$$\Delta E_H = E_L - E_H \quad (15)$$

$$\Delta E_B = E_H - E_B \quad (16)$$

2.4.4 Statistical analysis

The curve regression analysis method was employed to determine the quantitative relations between hydraulic characteristics, jet properties, runoff energy consumption and soil erosion rate and inflow discharge. The fitted equations between soil loss rate of three landform units and hydraulic characteristics, jet properties, and energy consumption were also quantified by the curve regression. The soil erosion volume of upstream area, gully head and gully bed were derived from the DEM of different stages through the ArcGIS 10.0 software. The data analyse was executed by using SPSS software (version 6.0) and figure plotting was carried out with Origin 8.5 and PowerPoint 2016 software.

3 Results

3.1 Spatial-temporal changes in jet properties and runoff hydraulic

3.1.1 Jet properties of gully head

Fig. 5 shows the temporal variation of three jet property parameters of gully head (GH) under different inflow discharge conditions. Overall, the flow velocity at the headcut brinkpoint (V_b) increased obviously in the first 30 min and then showed a gradually stable tendency with some degree of fluctuation (Fig. 5a), and the fluctuation degree was enhanced as the inflow discharge increased. For example, the V_b increased sharply from 0.66 to 0.88 m s^{-1} during 100 – 124 min under 6.0 m^3 h^{-1} inflow discharge due to the headwall failure near headcut enhancing the runoff turbulence. Regression analysis revealed the significant power relationships ($V_b=a \cdot t^b$, R^2=0.139-0.704, $P<0.01$) between V_b and time (t) (Table 1). Furthermore, except for 3.6 m^3 h^{-1} condition, the a-value increased with the inflow discharge increased, but the b-value showed a weak variation (0.08 - 0.10), indicating that the flow drainage from gully head could improve initial V_b but not change its trend over time. The mean V_b exhibited a significantly exponential relationship with inflow discharge (Fig. 5b, $P<0.05$). Contrary to the V_b, the jet velocity entry to plunge pool (V_e) and the jet shear stress (τ_j) experienced a gradually decreased trend with time (Fig. 5c, 5e). Notably, the V_e and τ_j suddenly decreased at 120th min and lasted nearly 40 minutes under 3.0 m^3 h^{-1} inflow discharge, which was mainly attributed to the developed second headcut shortening the jet-flow height. The temporal change of V_e could be described by logarithmic functions under 3.0 – 4.8 m^3 h^{-1} inflow discharge, and expressed by linear functions under the other inflow discharges, whereas the decrease of the τ_j with time could be presented by logarithmic functions under all inflow discharge conditions (Table 1). Furthermore, both of mean V_e and τ_j could be expressed by a positive "*S*" function of inflow discharge (Fig. 5d, 5f).

3.1.2 Runoff regime of upstream area and gully bed

The temporal changes in runoff Reynold number (*Re*) and Froude number (*Fr*) of upstream area (UA) and gully bed (GB) and their relationships with inflow discharge are provided in Fig. 6. The *Re*

of UA and GB showed a similar trend over time, that is, the *Re* firstly increased in the first40 min and then gradually stabilized (Fig. 6a). In addition, the *Re* of UA was larger than that of GB at any time under same inflow discharge, indicating that the runoff turbulence became weaker after the runoff of UA passed the gully head. Regression analysis showed the temporal variation in *Re* of UA could be described by logarithmic and power functions, but, for the GB, the relationship was mainly dominated by power function (Table 2). On average, the *Re* of GB was 50.5% - 65.9% less than that of UA, and the *Re* of UA and GB both increased with the increase of inflow discharge as a power function (Fig. 6b). However, as illustrated in Fig. 6c, the *Fr* experienced a completely opposite trend to *Re*. The *Fr* of UA decreased in the first 60 min and then gradually stabilized, but the *Fr* of GB experienced a relatively weak-fluctuating variation over time. For the most of cases, the change in *Fr* of UA and GB over time could be expressed by logarithmic functions (Table 2). On average, the *Fr* of UA was 2.39-3.04 times that of GB for same inflow discharge, and the positive power function could describe the relationship between *Fr* and inflow discharge (Fig. 6d).

Furthermore, the knowledge of open channel hydraulics is adopted to investigate the difference in runoff regime between UA and GB. The specific definition is: the flow belongs to laminar when *Re* is less than 500, the flow is turbulent when *Re* is larger than 2000, and the flow indicates transitional when *Re* ranges from 500 to 2000; and $Fr = 1$ is the critical value for to distinguish the subcritical and supercritical flow. The six flow regime zones were divided by three boundary lines ($Re = 500$, $Re = 2000$, and $Fr = 1$) according to the logarithmic relationship between the flow velocity and hydraulic radius (Fig. 7) (Xu et al., 2017b; Guo et al., 2020b). AS shown, the runoff regimes of UA and GB were located in entirely different zones. The flow of UA was in the supercritical-transition flow regime in the first 26 min and then gradually transformed to supercritical-turbulent flow regime under 3.0 – 6.0 m^3 h^{-1} inflow discharge, but the flow at any moment was in the supercritical-turbulent regime zone under 7.2 m^3 h^{-1} inflow discharge. Moreover, the higher inflow discharge would enhance the flow turbulent degree. The flow of GB belonged to subcritical-laminar flow category in the initial 6 min, and then transformed to subcritical-transition and subcritical-turbulent flow regime when inflow discharge was 3.0 and 3.6 m^3 h^{-1}. The flow was in the subcritical-turbulent flow regime in most of experimental duration when the inflow discharge is

4.8 – 7.2 m^3 h^{-1}. The difference in flow regime between UA and GB also indicated that the presence of gully head can greatly reduce flow turbulence.

3.1.3 Runoff shear stress and stream power of upstream area and gully bed

Fig.8 shows the temporal changes in runoff shear stress (τ) and stream power (ω) of upstream area (UA) and gully bed (GB) and their relationships with inflow discharge. Overall, the τ of UA and GB exhibited a gradually increased trend in the first 60 min, and whereafter, a relative steady state was obtained, but the larger inflow discharge perturbed the steady situation (Fig. 8a). Furthermore, the temporal change in τ of UA could be expressed by logarithmic functions, and the τ of GB showed a significant power function with experimental time (Table 2). On average, the τ of GB was 2.8% - 15.7% larger than the UA. The averaged τ of UA and GB increased with inflow discharge as a power function ($\tau=a-b/q$), and the GB had a faster increased-speed (b-value) than UA (Fig. 8b), signifying that the difference in τ between UA and GB would be widened with the inflow discharge increased. Similarly, the ω of UA and GB also exhibited a trend of gradual increase and stabilization over time (Fig. 8c). Different from the temporal change in τ, the ω of GB was always less than that of UA at any time for all inflow discharge conditions. Likewise, the variation in ω of UA and GB over time exhibited a significant logarithmic and power function, respectively. On average, the ω of GB was 49.2% - 65.9% less than UA, and the positive increase in ω of UA and GB with the inflow discharge could be expressed by a power function (Fig. 8d).

3.2 Spatial-temporal change of energy consumption

Fig. 9 illustrates the temporal change in accumulated energy consumption of upstream area (UA), gully head (GH) and gully bed (GB). The accumulated energy consumption of the three landform units continued to linearly increase with time (R^2=0.990-0.999, $P<0.01$), of which the accumulated energy consumption in GH was always the highest at any time, followed by UA and GB for the experiments of five inflow discharges. Moreover, the energy consumption rate (the slope-value of fitted equation) in the three landform units is basically constant, indicating the spatial-temporal change in energy consumption maintained a relatively steady state during gully

373 headcut erosion. Moreover, the energy consumption rate of GH was the highest, followed by UA and
374 GB, and the energy consumption rate in the three landform units also increased with the increase of
375 inflow discharge.

376 The variations of total energy consumption of UA, GH and GB and their proportions with
377 inflow discharge are shown in Fig. 10. As illustrated in Fig. 10a, both of the total energy
378 consumption of the "UA-GH-GB" system and the three landform units increased with the increase of
379 inflow discharge. When inflow discharge increased from 3.0 to 7.2 m^3 h^{-1}, the total energy
380 consumption of the system, UA, GH and GB increased by 3.6% - 105.3%, 3.4% - 62.0%, 3.5% -
381 108.2% and 9.0% - 327.5%, respectively. Regression analysis revealed that the energy consumption
382 of system and the three landform units increased with inflow discharge as an exponential function
383 ($y=a\cdot\exp(b\cdot x)$, a=1.14 - 55.41, b=0.13 - 0.36, R^2=0.954 - 0.992, P<0.05). Furthermore, in view of the
384 proportion of energy consumption, the energy consumption of UA accounted for 15.6% - 19.8% of
385 total energy consumption, and linearly decreased with inflow discharge increased (R^2=0.933,
386 $P<0.05$), whereas the proportion in GB (2.8% - 5.8%) linearly increased with inflow discharge
387 increased (R^2=0.983, P<0.05). However, the proportion of energy consumption (77.3% - 78.6%) in
388 GH showed a weak change with inflow discharge (Fig. 10b), signifying that the most of runoff
389 energy (77.5% on average) was consumed in the gully head position during headcut migration.
390

391 ## 3.3 Spatial-temporal change of soil loss

392 ### 3.3.1 Soil loss process

393 Fig. 11a shows that the soil loss rate of the "upstream area (UA)—gully head (GH)—gully bed
394 (GB)" system rose to a peak in first 20 min, then gradually descend and levelled off. Especially for
395 the 6.0 and 7.2 m^3 h^{-1}, the soil loss rate showed a severe fluctuation trend in the first 30 min. The
396 peak soil loss rate increased from 75.4 to 306.9 g s^{-1} with increasing inflow discharge. The soil loss
397 of UA and GH experienced a similar change process. The soil loss rate was the highest in the early
398 stage of the experiment, and gradually decreased with time, and became stable after 120 min (Fig.
399 11b, 11c). Furthermore, the temporal variation in soil loss of UA and GH could be well expressed by
400 logarithmic function ($S_L=a-b\cdot\ln(t)$, $P<0.05$, Table 3), and the a-value (representing initial soil loss

rate) and *b*-value (reflecting the reduction rate of soil loss rate with time) increased with increasing inflow discharge, indicating that larger inflow discharge can improve initial soil loss of UA and GH and also expedite the decrease of soil loss rate.

However, the GB presented a completely different soil loss process from UA and GH (Fig. 11d). The GB was always characterized by sediment deposition during the whole experiment for the 3.0 – 4.8 m^3 h^{-1} inflow discharges. The sediment deposition rate gradually decreased with time and presented a significant "S" function over time ($S_B=a/t-b$, R^2=0.918-0.982, P<0.01, Table 3). When the inflow discharge was larger than 4.8 m^3 h^{-1}, the sediment generated from UA and GH was deposited firstly in the GB and then gradually transported, and the temporal change of deposited sediment on GB accorded with logarithmic functions (R^2=0.936 and 0.906, P<0.01, Table 3). Furthermore, two critical time points (135 min and 111 min) can be derived from the two fitted logarithmic equations, which distinguished sediment deposition from sediment transport, signifying that the runoff began to transport the sediment deposited on GB after 135 min and 111 min for 6.0 and 7.2 m^3 h^{-1} inflow discharge.

3.3.2 Spatial distribution of soil loss

The variation in soil loss amount and proportion of the three landform units (UA, GH, GB) with inflow discharge is shown in Fig. 12. As illustrated in Fig. 12a, for the experiments of five inflow discharges, the soil loss was dominant in the UA and GH, but the GB was dominated by sediment deposition due to the weaker sediment transport capacity of runoff on GB than sediment deliverability of UA and GH. Furthermore, the soil loss amount of UA and GH ranged from 55.9 to 110.7 kg and from 310.0 to 994.8 kg, respectively, and increased linearly with increasing inflow discharge (R^2=0.966 and 0.969, P<0.05). The sediment deposition amount of GB ranged from 4.2 to 37.7 kg, and decreased with inflow discharge as a logarithmic function (R^2=0.961, P<0.05). In terms of proportion of soil loss (Fig. 12b), the proportion of UA and GH reached the maximum (15.3%) and minimum (84.7%), respectively under 3.0 m^3 h^{-1} inflow discharge, whereas, the proportion exhibited a little change (UA: 9.5% - 11.4%; GH: 88.6% - 90.5%) when the inflow discharge is 7.2 m^3 h^{-1},. Remarkably, the proportion of deposited sediment amount on GB to total soil loss amount

ranged from 0.4% to 10.3%, and decreased exponentially with inflow discharge (R^2=0.992, P<0.001).

3.4 Spatial change in hydrodynamic mechanism of soil loss

3.4.1 Relationships between soil loss and hydraulic parameters

Fig. 13 indicates the significant difference in the relationships between soil loss rate and hydraulic parameters among the three landform units (Fig. 13). For the upstream area (UA), the soil loss rate could be described as a series of exponential functions of runoff velocity, Reynold number, Froude number, runoff shear stress and stream power, of which the runoff shear stress and stream power showed a closer correlation with soil loss (Fig. 13a - 13e, R^2=0.830 – 0.945). Furthermore, the increased speed of soil loss rate obviously increased with the increasing hydraulic parameters (except for runoff velocity), indicating that soil loss of UA showed a stronger sensitive response to increasing hydraulic properties. However, the soil loss rate of gully bed (GB) linearly increased with the above-mentioned five parameters (Fig. 13f – 13j, R^2=0.918 – 0.994), which suggested that the decreased rate of sediment deposition of GB is basically constant with the increasing hydraulic properties. Further analysis showed that there are critical runoff velocity, Reynold number, Froude number, runoff shear stress and stream power for triggering the transformation of sediment deposition to soil erosion on GB, and the critical values are 0.26 m s^{-1}, 2845, 0.85, 6.94 Pa and 0.40 W m^{-2}, respectively. For the gully head (GH) position, the soil loss was significantly affected by jet velocity entry to plunge pool and jet shear stress (Fig. 13l and 13m, R^2=0.862 and 0.939), while the relationship between soil loss and flow velocity at the headcut brink-point was not significant (Fig. 13k, P=0.065).

3.4.2 Response of soil loss to energy consumption

As illustrated in Fig. 14, the soil loss rate of three landform units was positively and significantly related to the energy consumption (P<0.05), and a logarithmic function was found to fit the relationship between soil loss rate and energy consumption best (R^2=0.889 – 0.987). Furthermore, there is critical energy consumption to initiate soil erosion of the upstream area (UA) and gully head (GH) based on the fitted logarithmic functions (Fig. 14a, b). The critical energy consumption for GH

(5.79 J s^{-1}) is 2.57 times greater than that (1.62 J s^{-1}) of the UA. Similarly, for the gully bed (Fig. 14c), the minimum energy consumption (1.64 J s^{-1}) is needed to trigger the transformation of sediment deposition to soil loss.

4 Discussion

4.1 Spatial-temporal changes in hydraulic properties

This study revealed that the runoff velocity at the headcut brink-point (V_b) firstly raised and then gradually stabilized with time (Fig. 5a), which was closely corresponded to the gradually decreased runoff width on the upstream area with time (Shi et al., 2020a). However, this result was inconsistent with Zhang et al (2016, 2018) and Shi et al (2020b) who reported that the V_b decreased over time, which was mainly due to the gradually increased roughness and resistance of underlying surface over time reducing the runoff velocity (Su et al., 2015). The further analysis of power function between V_b and time ($V_b=a\cdot t^b$, Table 1) showed that the a-value increased but the b-value showed a weak variation with the inflow discharge increased, indicating that upstream flow can improve initial V_b but not affect its change trend over time. By contrast, the jet velocity entry to plunge pool (V_e) and jet shear stress (τ_j) experienced a gradually decreased process (Fig. 5c, 5e), which was mainly attributed to the shortening of jet-flow height caused by the development of second headcut and upstream flow undercutting headcut brink-point (Guo et al., 2019). This result, however, differed from the finding of Zhang et al. (2016) who stated the V_e and τ_j remained stable as the experiments progressed, which was mainly attributed to the weak change of jet-flow height induced by slow headcut retreat.

For the runoff hydraulic of upstream area (UA) and gully bed (GB), the Reynold number *Re* of UA and GB initially increased and gradually stabilized, but the Froude number *Fr* showed an opposite trend. This phenomenon was agreed with previous studies (e.g. Su et al., 2015; Zhang et al., 2016; Shi et al., 2020a). Besides, for the same upstream inflow discharge, the *Re* and *Fr* of UA were larger than that of GB by 50.5%-65.9% and 1.39-2.04 times, respectively, indicating that the runoff turbulence became weaker after the runoff of UA passed the gully head and plunge pool. More evidently, the runoff on UA was in the supercritical-transition and supercritical-turbulent flow regime ($Re > 500$, $Fr > 1$), whereas the runoff on GB belonged to subcritical-transition and subcritical-turbulent flow regime ($Re > 500$, $Fr < 1$). The above result was supported by Shi et al.

(2020a) who stated that the *Re* of gully bed decreased by 1.5%-30% as the flow fell from the upstream area, but Su et al. (2015) suggested that the steady state *Re* of gully bed was higher than that of upstream area. In the study of Su et al. (2015), the larger gully bed slope gradient than upstream area would accelerate the runoff velocity and thus enhance flow turbulence (Bennett, 1999; Pan et al., 2016). Our study found that temporal variation in the shear stress (τ) and stream power (ω) of UA was similar with GB, and, compared to UA, the τ and ω of GB increased and decreased by 2.8% - 15.7% and 49.2% - 65.9%, respectively. This was different from some previous experimental studies on gully and bank gully. For example, the result from the study of Shi et al. (2020a) indicated that the τ of gully bed decreased by 65.9% - 67.1%, compared to catchment area, and a similar result was also found during bank gully headcut erosion (Su et al., 2015). Previous studies also have proven that the change in hydraulic properties from upstream area to gully bed is affected by various factors including plunge pool size, slope gradient, initial step height, and soil texture (Bennett and Casalí, 2001; Wells et al., 2009a, 2009b).

4.2 Spatial-temporal change in runoff energy consumption and soil erosion

Our study revealed that the accumulated runoff energy consumption of the upstream area (UA), gully headcut (GH) and gully bed (GB) linearly increased over time (Fig. 9), indicating the spatial-temporal change in energy consumption maintained a relatively steady state during gully headcut erosion. However, the flow energy consumption of bank gully in three landform units logarithmically increased over time (Su et al., 2015). This difference further manifested that the runoff energy consumption of different landform units depends on gully type to some extent as well as soil texture, slope and headwall height (Wells et al., 2009a). Besides, under this flow discharge conditions, the proportion of energy consumption in UA, GH and GB was 15.6%-19.8%, 77.3%-78.6% and 2.8%-5.8%, respectively (Fig. 10), which was also indirectly supported by the study of Su et al. (2015) who suggested that the runoff energy consumption per unit soil loss from upstream area, headcut and gully bed is 17.4%, 70.5% and 12.0%, respectively. This further signified that the gully head consumed the most of runoff energy (77.5% on average) during headcut migration. The flow energy must be consumed to surmount the soil resistance as headcut migrates, and the consumed energy was mainly focused on headwall and plunge pool development (Alonso et

al., 2002).

In terms of soil loss, our study indicated that the soil loss rate of the "UA-GH-GB" system initially increased to the peak value and then gradually declined and stabilized (Fig. 11), which was consistent with the results of many studies on rill and gully headcut erosion under different conditions (slope, initial step height, flow discharge, soil type, soil stratification) (Bennett, 1999; Bennett and Casalí, 2001; Gordon et al., 2007; Wells et al., 2009a; Shi et al., 2020a). Both the scour depth and sediment production increased in the initial period of underlying surface adjustment, while once the plunge pool development was maintained, and sediment yield decreased and gradually stabilized (Bennett et al., 2000). In addition, the significant difference in soil loss process was found among the three landform units. The soil loss of UA and GH decreased logarithmically over time, which was similar with several studies (e.g. Su et al., 2015; Shi et al., 2020b). Nevertheless, the GB was always characterized by sediment deposition for the inflow discharge of < 4.8 m^3 h^{-1}, whereas the sediment was deposited firstly and then gradually transported as the inflow discharge increased to 6.0 and 7.2 m^3 h^{-1}. Similar results were also found in some previous studies on rill heacut erosion (Bennett, 1999; Bennett and Casalí, 2001; Gordon et al., 2007; Wells et al., 2009a). However, Su et al. (2014, 2015) revealed a larger soil loss volume or soil loss rate in gully bed than upstream area and headwall during bank gully headcut erosion. This difference between our study and Su et al. (2014, 2015) is primarily caused by the difference in slope gradient. The gully bed slope (20°) of bank gully was larger than that (3 °) of our study, indicating the runoff on gully bed of bank gully had stronger sediment transport capacity (Zhang et al., 2009; Ali et a., 2013; Wu et al., 2016, 2018). In view of the proportion of soil loss, the proportion of UA and GH was 9.5% - 11.4% and 88.6% - 90.5%, respectively, of which the proportion of deposited sediment on GB to the sediment yield from UA and GH can reach up to 0.4% - 10.3%. This result fully demonstrated that the gully head is the main source of sediment production during gully headcut erosion (Oostwoud-Wijdenes & Bryan, 1994; Zhao, 1994; Su et al., 2014), and also manifested the necessary and importance of gully headcut erosion controlling in gully-dominated region.

4.3 Hydrodynamic characteristics of headcut erosion

The significant different relationships between soil loss and jet or hydraulic characteristics was

found among UA, GH, and GB. The soil loss rate of UA exponentially increased with five hydraulic parameters (runoff velocity, Reynold number, Froude number, runoff shear stress and stream power), indicating that soil loss of UA showed a stronger sensitive response to increasing hydraulic properties. This could attribute to the frequent bank collapse on UA accelerating soil loss (Wells et al., 2013; Qin et al., 2018). However, the sediment deposition rate of GB linearly decreased with the five hydraulic parameters, signifying that sediment deposition on GB decreased at a stable state with the increase of hydraulic parameters. Therefore, the sediment deposition rate would reach zero when the five hydraulic parameters increased to the critical values, implying that the transformation of sediment deposition to sediment transport on GB would be triggered. Furthermore, the shear stress is the optimal parameter describing soil loss process of UA and GB, which differed from some studies on hillslope erosion hydrodynamic characteritics (Zhang et al., 2009; Shen et al., 2019; Ma et al., 2020). Most of studies have verified that stream power is the superior hydrodynamic parameter describing soil detachment process. This comparison also fully illustrated the great difference in hydrodynamic characteristic between hillslope erosion and headcut erosion. In this study, the soil loss of gully head (including plunge pool erosion) was significantly affected by jet properties. It's confirmed that the plunge pool erosion by jet flow becomes a crucial process controlling gully head migration and sediment production (Oostwoud-Wijdenes et al., 2000). Consequently, the plunge pool erosion theory is usually employed to build several headcut retreat models (Alonso et al., 2002; Campo-Bescós et al., 2013). Although the weak correlation between soil loss of gully head and flow velocity at headcut breakpoint, the larger flow velocity resulted from increasing inflow discharge would improve the shear stress of jet flow impinging gully bed, and thus the gully headcut suffered stronger incisional erosion of the plunge pool. However, in fact, the soil loss of gully head was also affected by on-wall flow erosion (Chen et al., 2013), and thus more studies should be conducted to clear the effect of on-wall flow properties on headcut erosion.

From the energy consumption perspective, the soil loss rate of the three landform units significantly and logarithmically increased with the energy consumption, and the similar change trend was also found in the study of Su et al. (2015). This finding suggests that energy consumption could be considered as the available parameter to estimate the soil loss of gully headcut erosion (Shi

et al., 2020b). Furthermore, we found the critical energy consumption initiating soil erosion of UA, GH, and GB are 1.62 J s^{-1}, 5.79 J s^{-1} and 1.64 J s^{-1}, respectively, indicating the soil loss of gully head (including plunge pool) needs more flow energy consumption (Zhang et al., 2018; Shi et al., 2020a, 2020b). This phenomenon can be attributed to the fact that the more runoff energy was consumed at the gully headwall and plunge pool erosion than UA and GB and thus resulted in more severe soil loss during headcut erosion.

Summary

This study investigated the temporal-spatial changes in flow hydraulic, energy consumption and soil loss during headcut erosion based on a series of scouring experiments of gully headcut erosion. The jet properties of gully head (GH) were significantly affected by upstream flow discharge. The upstream area (UA) and gully bed (GB) had similar temporal changes in Reynold number, Froude number, shear stress and stream power. The flow was supercritical on UA, but subcritical on GB, and the turbulent degree was enhanced by the increasing inflow discharge. The flow Reynold number, shear stress and stream power decreased by 56.0%, 63.8% and 55.9%, respectively, but Froude number increased by 7.9% when flow passed the gully headcut and plunge pool. The accumulated energy consumption at UA, GH and GB linearly increased with time, of which the GH consumed 77.5% of the total runoff energy. The soil loss of UA and GH decreased logarithmically over time, whereas the GB was mainly characterized by sediment deposition. The GH can contribute 88.5% of total soil loss, of which 3.8% sediment production was deposited on GB. The soil loss of UA and GH and the sediment deposition of GB were significantly affected by hydraulic and jet properties. Our study revealed that the critical energy consumption to initiate soil erosion of UA, GH and GB are 1.62 J s^{-1}, 5.79 J s^{-1} and 1.64 J s^{-1}, respectively. The runoff energy consumption could be considered as a non-negligible parameter to predict soil loss of gully headcut erosion.

Data availability

At present, the data are not publicly accessible because of a situation that we don't have permission to share data according to the requirement of the funded program and our institute.

Author contribution

Mingming Guo and Wenlong Wang designed the experiments. Mingming Guo, Zhuoxin Chen, Tianchao Wang, Qianhua Shi, Man Zhao and Lanqian Feng carried out the experiments. Zhuoxin Chen produced and processed the digital elevation model of erosion landform. Mingming Guo and Wennlong Wang written and prepared the manuscript with contributions from all co-authors.

Competing interests:

The authors declare that they have no conflict of interest.

Acknowledgments

This work was supported by the National Natural Science Foundation of China (41571275) and the National Key Research and Development Program of China (2016YFC0501604). Acknowledgement for the data support from "Loess Plateau Data Center, National Earth System Science Data Sharing Infrastructure, National Science & Technology Infrastructure of China. (http://loess.geodata.cn)".

References

Addisie, M.B., Ayele, G.K., Gessess, A.A., Tilahun, S.A., Zegeye, A.D., Moges, M.M., … Steenhuis, T.S.: Gully head retreat in the sub-humid Ethiopian Highlands: The Ene-Chilala catchment, Land Degradation & Development, 28, 1579–1588, https://doi.org/10.1002/ldr.2688, 2017.

Ali, M., Seeger, M., Sterk, G., Moore, D.: A unit stream power based sediment transport function for overland flow. Catena. 101, 197-204. https://doi.org/10.1016/j.catena.2012.09.006

Alonso, C.V., Bennett, S.J., Stein, O.R., 2002. Predicting head cut erosion and migration in concentrated flows typical of upland areas, Water Resources Research, 38, 39-1–39-15, http://dx.doi.org/10.1029/2001WR001173, 2013.

Beer, C.E., Johnson, H.P.: Factors in gully growth in the deep loess area of western Iowa. Transactions of ASAE, 6, 237–240, https://doi.org/10.13031/2013.40877, 1963.

Bennett, S.J., Casali, J.: Effect of initial step height on headcut development in upland concentrated flows. Water Resources Research, 37, 1475–1484, https://doi.org/10.1029/2000WR900373, 2001.

Bennett, S.J.: Effect of slope on the growth and migration of headcuts in rills, Geomorphology, 30, 273–290, https://doi.org/10.1016/S0169-555X(99)00035-5, 1999.

Bennett, S.J., Alonso, C.V.: Turbulent flow and bed pressure within headcut scour holes due to plane reattached jets, Journal of Hydraulic Research, 44, 510–521, https://doi.org/10.1080/00221686.2006.9521702, 2006.

626 Bennett, S.J., Alonso, C.V., Prasad, S.N., Romkens, M.J.: Experiments on headcut growth and migration in
627 concentrated flows typical of upland areas, Water Resources Research, 36, 1911–1922,
628 https://doi.org/10.1029/2000WR900067, 2000.
629 Campo-Bescós, M.A., Flores-Cervantes, J.H., Bras, R.L., Casalí, J., Giráldez, J.V.: Evaluation of a gully
630 headcut retreat model using multitemporal aerial photographs and digital elevation models, Journal of
631 Geophysical Research: Earth Surface, 118, 2159–2173, https://doi.org/10.1002/jgrf.20147, 2013.
632 Chaplot, V., Giboire, G., Marchand, P., Valentin, C.: Dynamic modelling for linear erosion initiation and
633 development under climate and land-use changes in northern Laos, Catena, 63, 318–328,
634 https://doi.org/10.1016/j.catena.2005.06.008, 2005.
635 Che, X.L.: Study of distribution characteristic and evolution of headward erosion on Dongzhi tableland of the
636 loess gully region, Yangling: Northwest A&F University, pp. 66-67, (In Chinese), 2012.
637 Chen, A., Zhang, D., Peng, H., Fan, J., Xiong, D., Liu, G.: Experimental study on the development of collapse
638 of overhanging layers of gully in Yuanmou Valley, China, Catena, 109, 177-185,
639 https://doi.org/10.1016/j.catena.2013.04.002, 2013.
640 De Baets, S., Poesen, J., Knapen, A., Galindo, P.: Impact of root architecture on the erosion-reducing potential
641 of roots during concentrated flow, Earth Surface Processes and Landforms, 32, 1323–1345,
642 https://doi.org/10.1002/esp.1470, 2007.
643 de Vente, J., Poesen, J.: Predicting soil erosion and sediment yield at the basin scale: Scale issues and
644 semi-quantitative models, Earth-Science Reviews, 71, 95–125, https://doi.org/10.1016/j.earscirev.2005.02.002,
645 2005.
646 DeLong, S.B., Johnson, J., Whipple, K.: Arroyo channel head evolution in a flash-flood–dominated
647 discontinuous ephemeral stream system, Geological Society of America Bulletin, 126, 1683–1701,
648 https://doi.org/10.1130/B31064.1, 2014.
649 Descroix, L., González Barrios, J.L., Viramontes, D., Poulenard, J., Anaya, E., Esteves, M., Estrada, J.: Gully
650 and sheet erosion on subtropical mountain slopes: their respective roles and the scale effect, Catena, 72,
651 325–339, https://doi.org/10.1016/j.catena.2007.07.003, 2008.
652 Dotterweich, M., Rodzik, J., Zglobicki, W., Schmitt, A., Schmidtchen, G., Bork, H.R.: High resolution gully
653 erosion and sedimentation processes, and land use changes since the Bronze Age and future trajectories in the
654 Kazimierz Dolny area (Nałęczów Plateau, SE-Poland), Catena, 95, 50–62,
655 https://doi.org/10.1016/j.catena.2012.03.001, 2012.
656 Flores-Cervantes, J., Istanbulluoglu, E., Bras, R.: Development of gullies on the landscape: A model of
657 headcut retreat resuUAing from plunge pool erosion, Journal of Geophysical Research, 111, 1–14,
658 https://doi.org/10.1029/2004JF000226, 2006.
659 Frankl, A., Stal, C., Abraha, A., Nyssen, J., Rieke-Zapp, D., DeWulf, A., Poesen, J.: Detailed recording of
660 gully morphology in 3D through image-based modelling, Catena, 127, 92–101,
661 https://doi.org/10.1016/j.catena.2014.12.016, 2015.
662 Fu, B.J., Liu, Y., Lv, Y.H., He, C.S., Zeng, Y., Wu, B.F.: Assessing the soil erosion control service of
663 ecosystems change in the Loess Plateau of China, Ecological Complexity, 8, 284-293,
664 https://doi.org/10.1016/j.ecocom.2011.07.003, 2011.
665 Gordon, L.M., Bennett, S.J., Wells, R.R., Alonso, C.V.: Effect of soil stratification on the development and
666 migration of headcuts in upland concentrated flows, Water Resources Research, 43, W07412,
667 https://doi.org/10.1029/2006WR005659, 2007.

Guo, M., Wang, W., Shi, Q., Chen, T., Kang, H., Li, J.: An experimental study on the effects of grass root density on gully headcut erosion in the gully region of China's Loess Plateau, Land Degradation & Development, 30, 2107–2125, https://doi.org/10.1002/ldr.3404, 2019.

Guo, M., Wang, W., Wang, T., Wang, W., Kang, H.: Impacts of different vegetation restoration options on gully head soil resistance and soil erosion in loess tablelands, Earth Surface Processes and Landforms, 45(4), 1038-1050, https://doi.org/10.1002/esp.4798, 2020.

Guo, M.M., Wang, W.L., Kang, H.L., Yang, B.: Changes in soil properties and erodibility of gully heads induced by vegetation restoration on the Loess Plateau, China, Journal of Arid Land, 10(5), 712-725, https://doi.org/10.1007/s40333-018-0121-z, 2018.

Guo, M.M., Wang, W.L., Li, J.M., Bai, Y., Kang, H.L., Yang, B.: Runoff characteristics and soil erosion dynamic processes on four typical engineered landforms of coalfields: An in-situ simulated rainfall experimental study, Geomorphology 349, 106896, https://doi.org/10.1016/j.geomorph.2019.106896, 2020.

Hager, W.H.: Hydraulics of plane free overfall, Journal of Hydraulic Engineering, 109, 1683–1697, https://doi.org/10.1061/(ASCE)0733-9429(1983)109:12(1683) , 1983.

Hanson, G.J., Robinson, K.M., Cook, K.R.: Prediction of headcut migration using a deterministic approach, Transactions of the ASAE, 44(4), 525-531, https://doi.org/10.13031/2013.6112, 2001.

Hosseinalizadeh, M., Kariminejad, N., Chen, W., Pourghasemi, H.R., Alinejad, M., Behbahani, A.M., Tiefenbacher, J.P.: Gully headcut susceptibility modeling using functional trees, naïve Bayes tree, and random forest models, Geoderma, 342, 1-11, https://doi.org/10.1016/j.geoderma.2019.01.050, 2019.

Ionita, I.: Gully development in the Moldavian Plateau of Romania, Catena, 68, 133–140, https://doi.org/10.1016/j.catena.2006.04.008, 2006.

Ionita, I., Niacsu, L., Petrovici, G., Blebea-Apostu, A.M.: Gully development in eastern Romania: a case study from Falciu Hills, Natural Hazards, 79, 113–138, https://doi.org/10.1007/s11069-015-1732-8, 2015.

Jiao, J.Y., Wang, W.Z., Hao, X.P.: Precipitation and erosion characteristics of rainstorm in different pattern on Loess Plateau, Journal of Arid Land Resources and Environment, 13(1), 34-42, (In Chinese), 1999.

Kirkby, M.J., Bull, L.J., Poesen, J., Nachtergaele, J., Vandekerckhove, L.: Observed and modelled distributions of channel and gully heads—with examples from SE Spain and Belgium, Catena, 50, 415–434, https://doi.org/10.1016/S0341-8162(02)00128-5, 2003.

Li, Binbing., Huang, Lei., Feng, Lin., Li, Peng., Yao, Jingwei., Liu, Fangming., Li, Junli., Tang, Hui.: Gully sidewall expansion process on loess hill slope erosion, Journal of Basic Science and Engineering, 24(6), 1147-1158. (In Chinese), 2016.

Li, H., Cruse, R.M., Liu, X.B., Zhang, X.Y.: Effects of topography and land use change on gully development in typical Mollisol region of Northeast China, Chinese Geographical Science, 26, 779-788, https://doi.org/10.1007/s11769-016-0837-7, 2016.

Li, M., Song, X.Y., Shen, B., Li, H.Y., Meng, C.X.: Influence of vegetation change on producing runoff and sediment in gully region of Loess Plateau, Journal of Northwest Sci-Tech University of AgricuUAure and Forestry (Natural Science Edition), 34, 117-120, (In Chinese), 2006.

Li, Z., Zhang, Y., Zhu, Q., He, Y., Yao, W.: Assessment of bank gully development and vegetation coverage on the Chinese Loess Plateau, Geomorphology, 228, 462–469, https://doi.org/10.1016/j.geomorph.2014.10.005, 2015.

Li, Z., Zheng, F.L., Liu, W.Z., Flanagan, D.C.: Spatial distribution and temporal trends of extreme temperature and precipitation events on the Loess Plateau of China during 1961–2007, Quaternary International, 226(1-2), 92-100, https://doi.org/10.1016/j.quaint.2010.03.003, 2010.

Ma, Q., Zhang, K., Cao, Z., Wei, M., & Yang, Z.: Soil detachment by overland flow on steep cropland in the subtropical region of China, Hydrological Processes, 34(8), 1810-1820, https://doi.org/10.1002/hyp.13694, 2020

Martínez-Casasnovas, J.A., Concepción Ramos, M., García-Hernández, David.: Effects of land‐use changes in vegetation cover and sidewall erosion in a gully head of the Penedès region (northeast Spain), Earth Surface Processes & Landforms, 34, 1927-1937, https://doi.org/10.1002/esp.1870, 2009.

Nazari Samani, A., Ahmadi, H., Mohammadi, A., Ghoddousi, J., Salajegheh, A., Boggs, G., Pishyar, R.: Factors Controlling Gully Advancement and Models Evaluation (Hableh Rood Basin, Iran), Water Resources Management, 24, 1532–1549, https://doi.org/10.1007/s11269-009-9512-4, 2010.

Oostwoud-Wijdenes, D., Bryan, R.B.: The significance of gully headcuts as a source of sediment on low-angle slopes at Baringo, Kenya, and initial control measures, Advances in Geoecology, 27, 205–231, 1994.

Oostwoud-Wijdenes, D., Poesen, J., Vandekerckhove, L., Ghesquiere, M.: Spatial distribution of gully head activity and sediment supply along an ephemeral channel in a Mediterranean environment, Catena, 39, 147–167, http://202.194.143.28:80/rwt/SD/https/MSYXTLUQPJUB/10.1016/S0341-8162(99)00092-2, 2000.

Pan, C., Ma, L., Wainwright, J., Shangguan, Z.: Overland flow resistances on varying slope gradients and partitioning on grassed slopes under simulated rainfall, Water Resources Research, 52, 2490–2512, https://doi.org/10.1002/2015WR018035, 2016.

Poesen, J., Nachtergaele, J., Verstraeten, G., Valentin, C.: Gully erosion and environmental change: Importance and research needs, Catena, 50, 91-133, https://doi.org/10.1016/S0341-8162(02)00143-1, 2003.

Qin, Chao., Zheng, Fenli., Wells Robert, R., Xu, Ximeng, Wang, Bin., Zhong, Keyuan.: A laboratory study of channel sidewall expansion in upland concentrated flows, Soil and Tillage Research, 178, 22-31, https://doi.org/10.1016/j.still.2017.12.008, 2018.

Reuter, H.I., Nelson, A., Jarvis, A.: An evaluation of void filling interpolation methods for SRTM data, International Journal of Geographic Information Science, 21(9), 983-1008, 2007.

Rieke-Zapp, D.H., Nichols, M.H.: Headcut retreat in a semiarid watershed in the southwestern United States since 1935, Catena, 87, 1–10, https://doi.org/10.1016/j.catena.2011.04.002, 2011.

Rodzik, J., Furtak, T., Zglobicki, W.: The impact of snowmeUA and heavy rainfall runoff on erosion rates in a gully system, Lublin Upland, Poland, Earth Surface Processes & Landforms, 34, 1938–1950, https://doi.org/10.1002/esp.1882, 2009.

Rouse, H.: Engineering hydraulics. Hoboken, NJ: Wiley, 1950.

Sanchis, M.P., Torri, D., Borselli, L., Poesen, J.: Climate effects on soil erodibility, Earth Surface Processes & Landforms, 33, 1082–1097, https://doi.org/10.1002/esp.1604, 2008.

Shen, N., Wang, Z., Zhang, Q., Chen, H., Wu, B.: Modelling soil detachment capacity by rill flow with hydraulic variables on a simulated steep loessial hillslope, Hydrology Research, 50(1), 85-98, https://doi.org/10.2166/nh.2018.037, 2018.

Shi, Q.H., Wang, W.L., Guo, M.M., Chen, Z.X., Feng, L.Q., Zhao, M., Xiao, H.: The impact of flow discharge on the hydraulic characteristics of headcut erosion processes in the gully region of the Loess Plateau, Hydrological processes, 34, 718-729, https://doi.org/10.1002/hyp.13620, 2020.

Shi, Q., Wang, W., Zhu, B., Guo, M.: Experimental study of hydraulic characteristics on headcut erosion and erosional response in the tableland and gully regions of China, Soil Science Society of America Journal, 84, 700–716, https://doi.org/10.1002/saj2.20068, 2020.

Stein, O., Julien, P., Alonso, C.: Mechanics of jet scour downstream of a headcut, Journal of Hydraulic Research, 31, 723–738, https://doi.org/10.1080/00221689309498814, 1993.

Su, Z.A., Xiong, D.H., Dong, Y.F., Zhang, B.J., Zhang, S., Zheng, X.Y., …Fang, H.D.: Hydraulic properties of concentrated flow of a bank gully in the dry‐hot valley region of southwest China, Earth Surface Processes and Landforms, 40, 1351‐1363. https://doi.org/10.1002/esp.3724, 2015.

Su, Z.A., Xiong, D.H., Dong, Y.F., Li, J.J., Yang, D., Zhang, J.H., He, G.X.: Simulated headward erosion of bank gullies in the Dry-hot Valley Region of southwest China, Geomorphology, 204, 532–541, https://doi.org/10.1016/j.geomorph.2013.08.033, 2014.

Sun, W.Y., Mu, X.M., Song, X.Y., Wu, D., Cheng, A.F., Qiu, B.: Changes in extreme temperature and precipitation events in the Loess Plateau (China) during 1960–2013 under global warming, Atmospheric Research, 168, 33-48, https://doi.org/10.1016/j.atmosres.2015.09.001, 2016.

Thompson, J.R.: Quantitative effect of watershed variables on rate of gully‐head advancement. Transactions of the ASABE, 7, 54‐55, https://doi.org/10.13031/2013.40694, 1964.

Torri, D., Poesen, J.: A review of topographic threshold conditions for gully head development in different environments, Earth-Science Reviews, 130, 73–85, https://doi.org/10.1016/j.earscirev.2013.12.006, 2014.

Valentin, C., Poesen, J., Li, Y.: Gully erosion: Impacts, factors and control, Catena, 63, 132–153, https://doi.org/10.1016/j.catena.2005.06.001, 2005.

Vandekerckhove, L., Poesen, J., Govers, G.: Medium-term gully headcut retreat rates in southeast spain determined from aerial photographs and ground measurements, Catena, 50(2-4), 329-352, https://doi.org/10.1016/S0341-8162(02)00132-7, 2003.

Vandekerckhove, L., Poesen, J., Wijdenes, D.O., Nachtergaele, J., Tomás de Figueiredo.: Thresholds for gully initiation and sedimentation in Mediterranean Europe, Earth Surface Processes & Landforms, 25(11), 1201-1220, https://doi.org/10.1002/1096-9837(200010)25:11<1201::AID-ESP131>3.0.CO;2-L, 2015.

Vanmaercke, M., Poesen, J., Mele, B.V., Demuzere, M., Bruynseels, A., Golosov, V., … Yermolaev, O.: How fast do gully headcuts retreat?, Earth‐Science Reviews, 154, 336‐355, https://doi.org/10.1016/j.earscirev.2016.01.009, 2016.

Vannoppen, W., Vanmaercke, M., De Baets, S., Poesen, J.: A review of the mechanical effects of plant roots on concentrated flow erosion rates, Earth‐Science Reviews, 150, 666‐678, https://doi.org/10.1016/j.earscirev.2015.08.011, 2015.

Vanwalleghem, T., Bork, H.R., Poesen, J., Schmidtchen, G., Dotterweich, M., Nachtergaele, J., Bork, H., Deckers, J., Brüsch, B., Bungeneers, J., De Bie, M.: Rapid development and infilling of a buried gully under cropland, Central Belgium, Catena, 63, 221–243, https://doi.org/10.1016/j.catena.2005.06.005, 2005.

Vanwalleghem, T., Van Den Eeckhaut, M., Poesen, J., Deckers, J., Nachtergaele, J., Van Oost, K., Slenters, C.: Characteristics and controlling factors of old gullies under forest in a temperate humid climate: a case study from the Meerdaal Forest (Central Belgium), Geomorphology, 56(1), 15–29, https://doi.org/10.1016/S0169-555X(03)00043-6, 2003.

Wells, R.R., Alonso, C.V., Bennett, S.J.: Morphodynamics of Headcut Development and Soil Erosion in Upland Concentrated Flows, Soil Science Society of America Journal, 73, 521–530. https://doi.org/10.2136/sssaj2008.0007, 2009a.

Wells, R.R., Bennett, S.J., Alonso, C.V.: Effect of soil texture, tailwater height, and pore‐water pressure on the morphodynamics of migrating headcuts in upland concentrated flows, Earth Surface Processes and Landforms, 34, 1867–1877, https://doi.org/10.1002/esp.1871, 2009b.

Wells, R.R., Momm, H.G., Rigby, J.R., Bennett, S.J., Bingner, R.L., Dabney, S.M.: An empirical investigation of gully widening rates in upland concentrated flows, Catena, 101, 114-121, https://doi.org/10.1016/j.catena.2012.10.004, 2013.

Wen, X., Wu, X., Gao, M.: Spatiotemporal variability of temperature and precipitation in Gansu province (northwest China) during 1951–2015, Atmospheric Research, 197, 132-149, https://doi.org/10.1016/j.atmosres.2017.07.001, 2017.

Wu, Bing., Wang, Zhanli., Zhang, Qingwei., Shen, Nan., Liu, June., Wang, Sha.: Evaluation of shear stress and unit stream power to determine the sediment transport capacity of loess materials on different slopes, Journal of Soil & Sediments, 18, 116–127, https://doi.org/10.1007/s11368-017-1758-5, 2018.

Wu, B., Wang, Z., Shen, N., Wang, S.: Modelling sediment transport capacity of rill flow for loess sediments on steep slopes, Catena, 147, 453-462, https://doi.org/10.1016/j.catena.2016.07.030, 2016.

Xia, L., Song, X.Y., Fu, N., Li, H.Y., Li, Y.L.: Impacts of land use change and climate variation on green water in the Loess Plateau Gully Region——A case study of Nanxiaohegou basin, Journal of Hydraulic Engineering, 48(6), 678-688, (In Chinese), 2017.

Xu, J.Z., Li, H., Liu, X.B., Hu, W., Yang, Q.N., Hao, Y.F., Zhen, H.C., Zhang, X.Y.: Gully Erosion Induced by SnowmeUA in Northeast China: A Case Study, Sustainability, 11, https://doi.org/10.3390/su11072088, 2019.

Xu. X.M., Zheng, F.L., Wilson, G.V., Wu, M.: Upslope inflow, hillslope gradient and rainfall intensity impacts on ephemeral gully erosion, Land Degradation & Development, 28, 2623-2635 https://doi.org/10.1002/ldr.2825, 2017.

Xu, X.M., Zheng, F.L., Qin, C., Wu, H.Y., Wilson, G.V.: Impact of cornstalk buffer strip on hillslope soil erosion and its hydrodynamic understanding, Catena, 149, 417–425, https://doi.org/10.1016/j.catena.2016.10.016, 2017.

Xu, X.M., Wang, H.B., Zhao, J.Y., Liu, X.J.: Dynamic variation of soil erosion of Nanxiaohegou small watershed during 2004-2016, Soil and Water Conservation in China, 443(2), 59-61, (In Chinese), 2019.

Zhang, B.J., Xiong, D.H., Su, Z.A., Yang, D., Dong, Y.F., Xiao, L., Zhang, S., Shi, L.T.: Effects of initial step height on the headcut erosion of bank gullies: a case study using a 3D photo-reconstruction method in the Dry-hot Valley region of southwest China, Physical Geography, 37, 409–429, https://doi.org/10.1080/02723646.2016.1219939, 2016.

Zhang, B.J., Xiong, D.H., Zhang G.H., Zhang, S., Wu, H., Yang, D., Xiao, L., Dong, Y.F., Su, Z.A., Lu, X.N.: Impacts of headcut height on flow energy, sediment yield and surface landform during bank gully erosion processes in the Yuanmou Dry‐hot Valley region, southwest China, Earth Surface Processes & Landforms, 43(10), 2271-2282, https://doi.org/10.1002/esp.4388, 2018.

Zhang, H.X.: The characteristics of hard rain and its distribution over the Loess Plateau, Acta Geographica Sinica, 38, 416–425, (In Chinese), 1983.

Zhang, G.H., Liu, Y.M., Han, Y.F., Zhang, X.C.: Sediment transport and soil detachment on steep slopes: I. transport capacity estimation, Soil Science Society of America Journal, 73, 1291-1297, https://doi.org/10.2136/sssaj2008.0145, 2009.

Zhao, A.C.: Analysis of control models of typical small watershed in gully area of Loess Plateau, the east part of Gansu Province, Research of Soil and Water Conservation, 1, 45–49, (In Chinese), 1994.

833 Zhu, T.X.: Gully and tunnel erosion in the hilly Loess Plateau region, China, Geomorphology, 153, 144–155,
834 https://doi.org/10.1016/j.geomorph.2012.02.019, 2012.

835 Table 1 The relationships between jet properties of gully headcut and time.

Inflow discharge (m^3 h^{-1})	V_b~t	V_e~t	τ_j~t
3.0	$V_b=0.42t^{0.09}$, $R^2=0.691^{**}$	$V_e=5.28-0.49\lg(t)$, $R^2=0.290^{**}$	$\tau_j=110.86-15.44\lg(t)$, $R^2=0.344^{**}$
3.6	$V_b=0.53t^{0.02}$, $R^2=0.139^{**}$	$V_e=4.52-0.17\lg(t)$, $R^2=0.859^{**}$	$\tau_j=117.93-13.14\lg(t)$, $R^2=0.823^{**}$
4.8	$V_b=0.46t^{0.08}$, $R^2=0.544^{**}$	$V_e=4.25-0.09\lg(t)$, $R^2=0.718^{**}$	$\tau_j=109.22-9.93\lg(t)$, $R^2=0.770^{**}$
6.0	$V_b=0.52t^{0.10}$, $R^2=0.509^{**}$	$V_e=4.17-1.33\times10^{-3}t$, $R^2=0.478^{**}$	$\tau_j=118.73-10.96\lg(t)$, $R^2=0.876^{**}$
7.2	$V_b=0.57t^{0.08}$, $R^2=0.704^{**}$	$V_e=4.09-1.38\times10^{-4}t$, $R^2=0.111^{**}$	$\tau_j=95.68-4.42\lg(t)$, $R^2=0.619^{**}$

836 Note: V_b, V_e and τ_j are runoff velocity at the headcut brinkpoint, runoff velocity entry to plunge pool and the jet
837 shear stress, respectively. ** refers to the significance of 0.01. The sample number is 90 for the fitted equations.
838

839 Table 2 Relationships between runoff hydraulic parameters and time.

Variable	Landform unit	Inflow discharge ($m^3\ h^{-1}$)				
		3.0	3.6	4.8	6.0	7.2
Reynold number	UA	Re=618.69lg(t) +286.69, R^2=0.761**	Re=705.93lg(t) +1006, R^2=0.815**	Re=1433lg(t) -1159, R^2=0.849**	Re=946.64$t^{0.38}$, R^2=0.794**	Re=2760$t^{0.14}$, R^2=0.486**
	GB	Re=514.36$t^{0.15}$, R^2=0.504**	—	Re=4.31t+1760, R^2=0.334**	Re=1.12×10$^3t^{0.16}$, R^2=0.566**	Re=744.99$t^{0.28}$, R^2=0.872**
Froude number	UA	Fr=2.89-0.33lg(t), R^2=0.651**	Fr=2.46-0.19lg(t), R^2=0.651**	Fr=3.27-0.35lg(t), R^2=0.656**	Fr=2.76-0.20lg(t), R^2=0.515**	—
	GB	Fr=0.72-0.05lg(t), R^2=0.326**	—	Fr=1.0-0.09lg(t), R^2=0.359**	—	Fr=1.21-0.10lg(t), R^2=0.634**
Shear stress	UA	τ=0.66lg(t)+0.55, R^2=0.737**	τ=1.18lg(t)+0.78, R^2=0.813**	τ=1.32lg(t)-0.62, R^2=0.817**	τ=1.50lg(t)-0.63, R^2=0.663**	τ=1.11lg(t)+0.99, R^2=0.819**
	GB	τ=2.44$t^{0.08}$, R^2=0.205**	τ=3.88$t^{0.05}$, R^2=0.106**	τ=2.27$t^{0.19}$, R^2=0.664**	τ=3.64$t^{0.12}$, R^2=0.212**	τ=1.99$t^{0.27}$, R^2=0.686**
Stream power	UA	ω=0.34lg(t)+0.16, R^2=0.761**	ω=0.38lg(t)+0.55, R^2=0.815**	ω=0.78lg(t)-0.63, R^2=0.849**	ω=0.69lg(t)-0.23, R^2=0.737**	ω=0.27lg(t)+1.56, R^2=0.436**
	GB	ω=0.28$t^{0.15}$, R^2=0.504**	ω=0.69$t^{0.09}$, R^2=0.123**	ω=0.50$t^{0.19}$, R^2=0.540**	ω=0.83$t^{0.09}$, R^2=0.338**	ω=0.51$t^{0.23}$, R^2=0.806**

840 Note: UA and GB refer to upstream area and gully bed. Re, Fr, τ and ω are Reynold number, Froude number, shear
841 stress, stream power, respectively. ** refers to the significance of 0.01. The sample number is 90 for the fitted
842 equations.
843

844 Table 3 Relationships between soil loss rate of three landform units and time

Inflow discharge (m^3 h^{-1})	Fitted equations		
	Upstream area	Gully head	Gully bed
3.0	S_L=15.71-2.34ln(t), R^2=0.909**	S_H=87.12-12.99ln(t), R^2=0.908**	S_B=-182.62/t-1.01, R^2=0.980**
3.6	S_L=23.97-4.18ln(t), R^2=0.938**	S_H=191.82-33.44ln(t), R^2=0.939**	S_B=-64.46/t-1.36, R^2=0.918**
4.8	S_L=28.76-4.85ln(t), R^2=0.930**	S_H=273.64-46.17ln(t), R^2=0.929**	S_B=-109.36/t-0.22, R^2=0.982**
6.0	S_L=44.0-7.69ln(t), R^2=0.884*	S_H=341.59-59.74ln(t), R^2=0.885*	S_B=2.03ln(t)-9.96, R^2=0.936**
7.2	S_L=47.34-8.25ln(t), R^2=0.922**	S_H=425.24-74.07ln(t), R^2=0.924**	S_B=1.86ln(t)-8.76, R^2=0.906**

845 Note: S_L, S_H and S_B are the soil loss rate of upstream area, gully head and gully bed, respectively. The sample No. is
846 6 for fitting equation. * and ** indicate the significant level of 0.05 and 0.01.
847

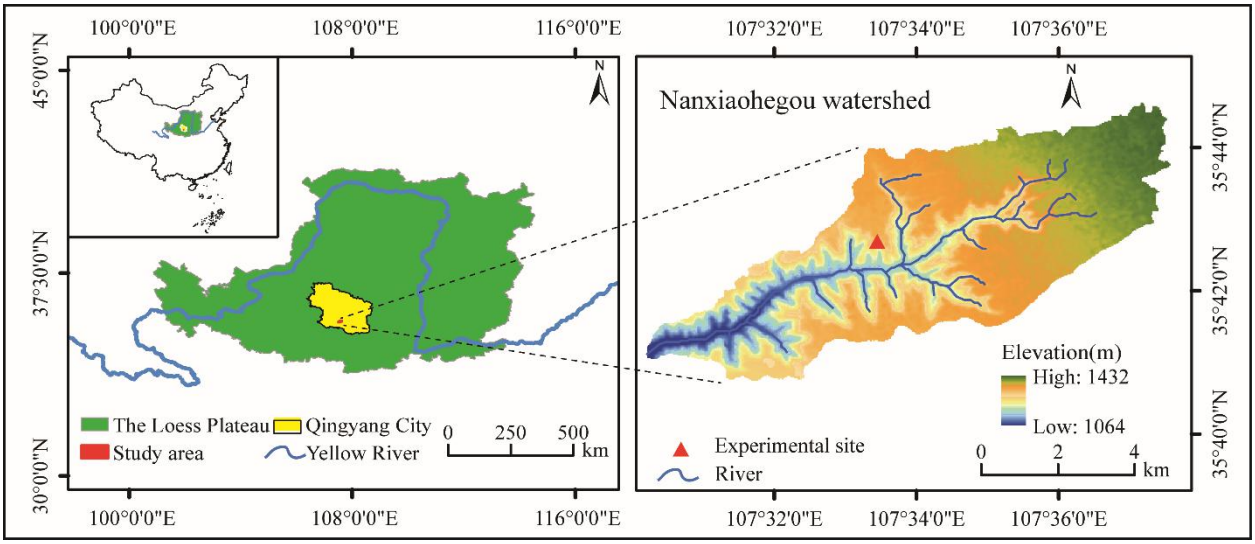

Figure 1 The location of the experimental site in Nanxiaohegou watershed, Qingyang City, Loess Plateau, China. Note: The figure production was based on the digital elevation model data (spatial resolution of 30 m) which is available from http://srtm.csi.cgiar.org (Reuter et al., 2007).

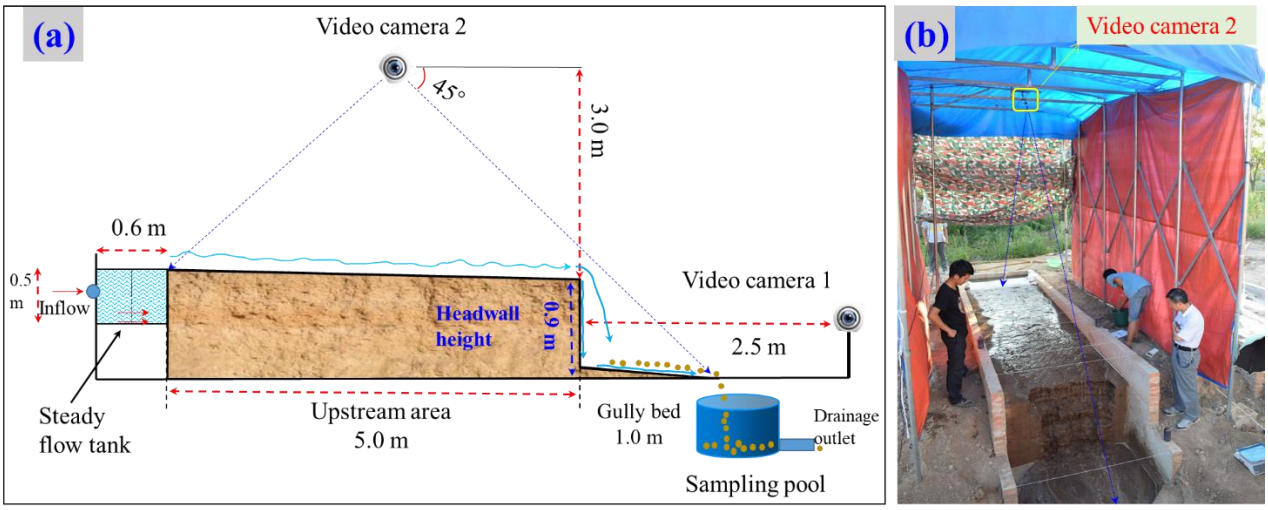

Fig.2 Sketch (a) and photo (b) of experimental plot.

Fig. 3 Runoff and sediment observation and recoding at upstream area, gully head and gully bed.

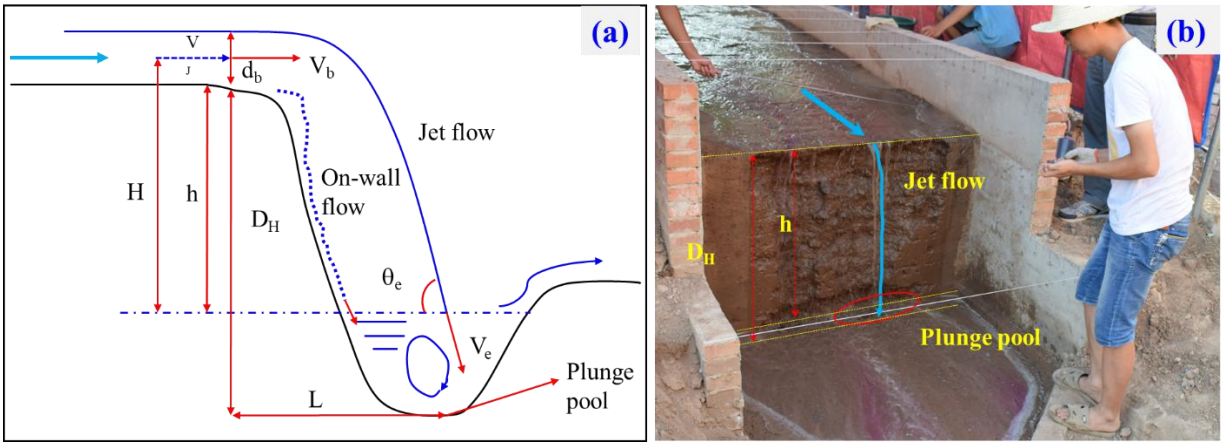

Fig. 4 Sketch of jet flow at gully headcut and plunge pool at gully bed.

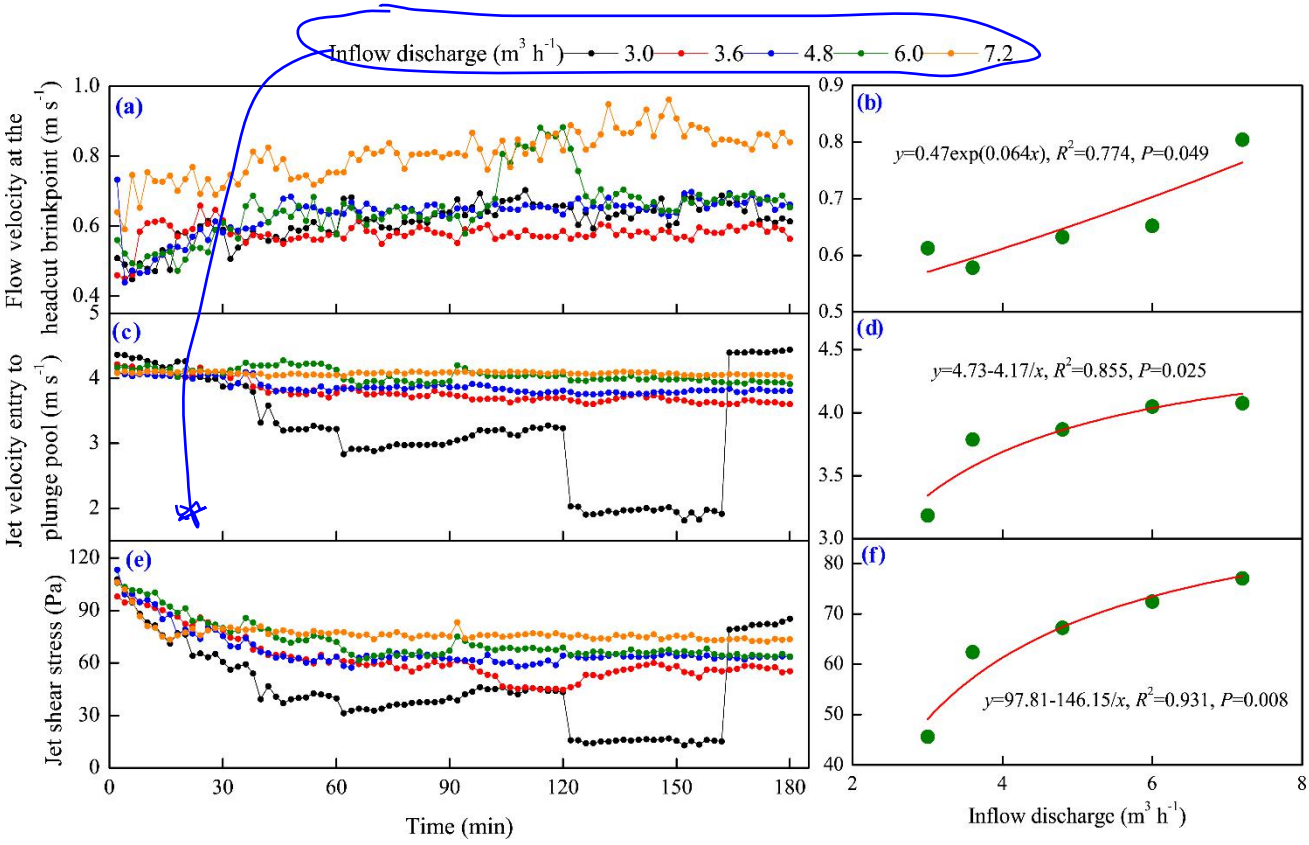

863

864 Fig.5 Temporal changes in jet properties of headcut and their relationships with inflow discharge.

865

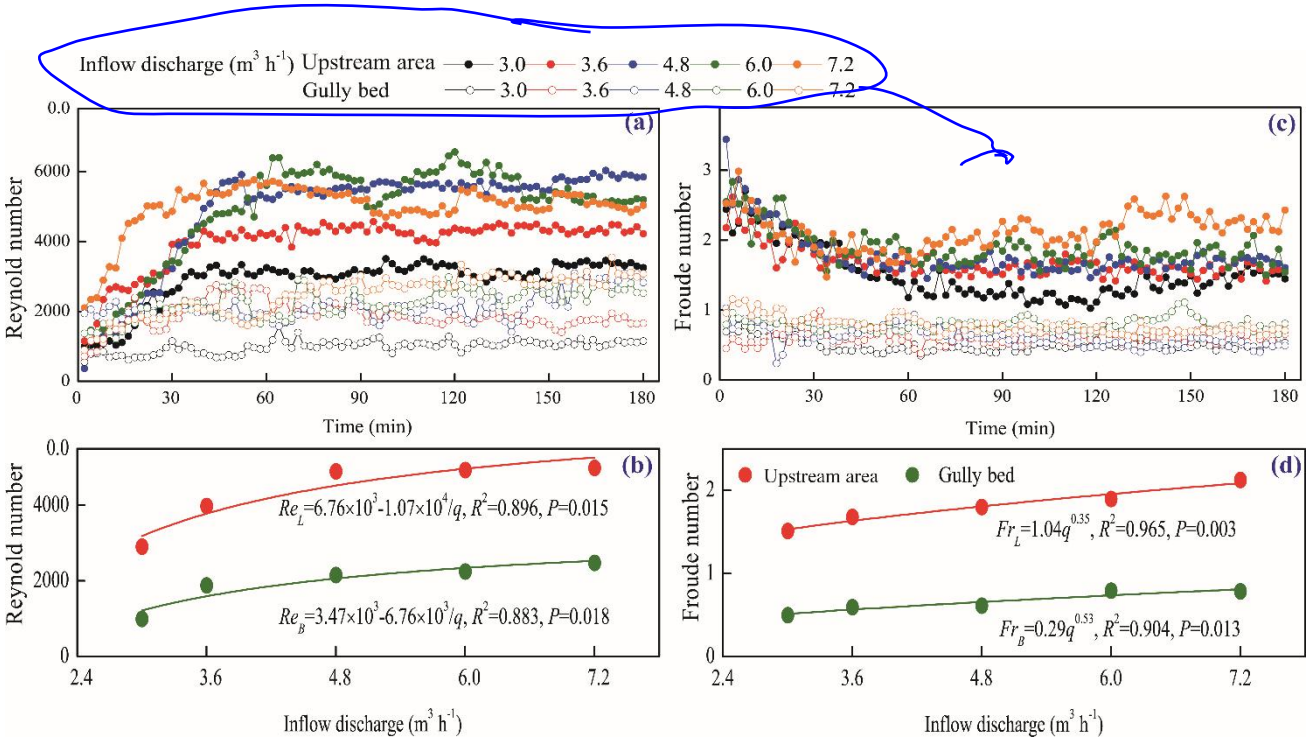

Fig.6 Temporal changes in runoff regime of upstream area and gully bed and their relationships with inflow discharge.

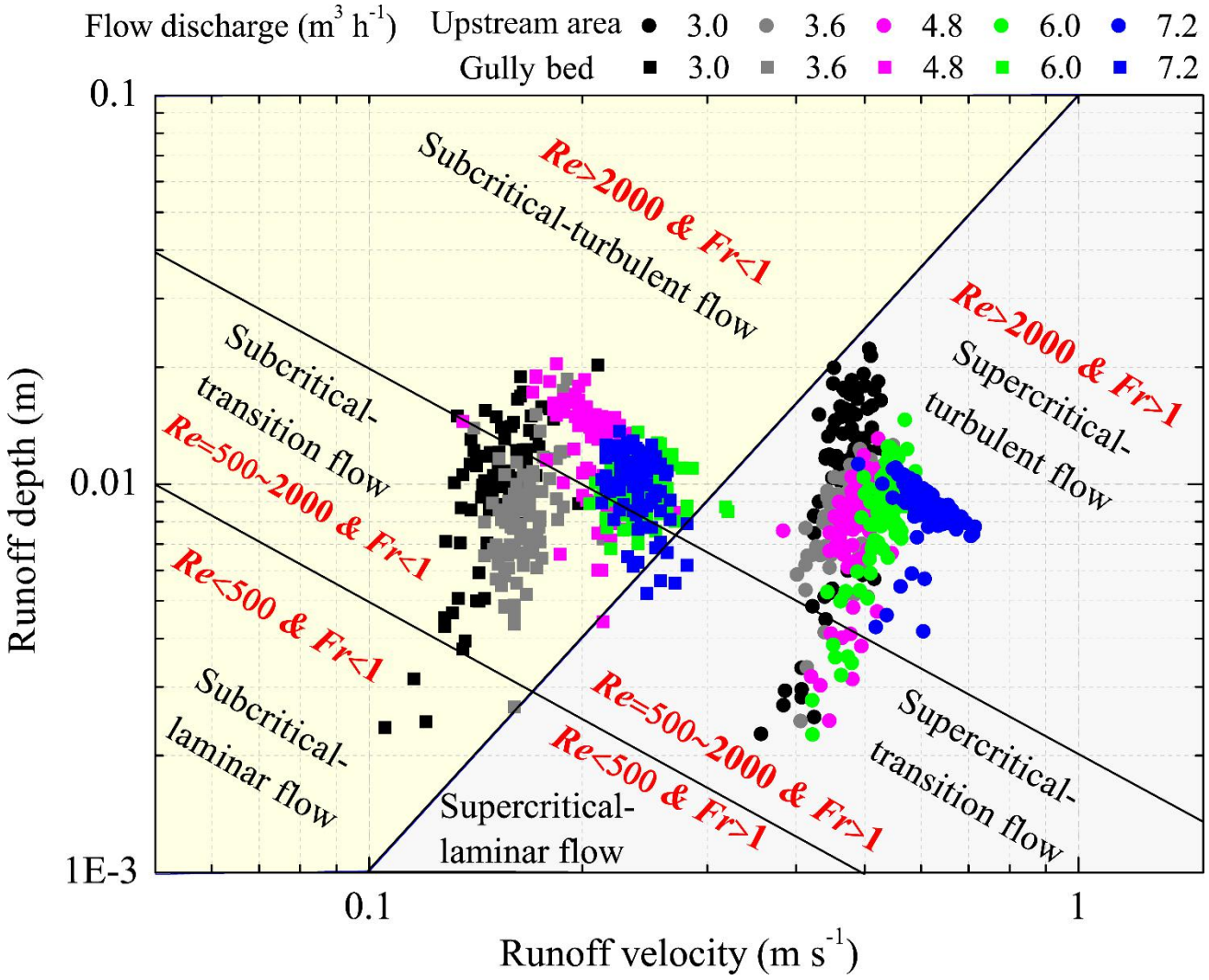

870

871 Fig. 7 Runoff regime zones of upstream area and gully bed under different inflow discharge conditions.

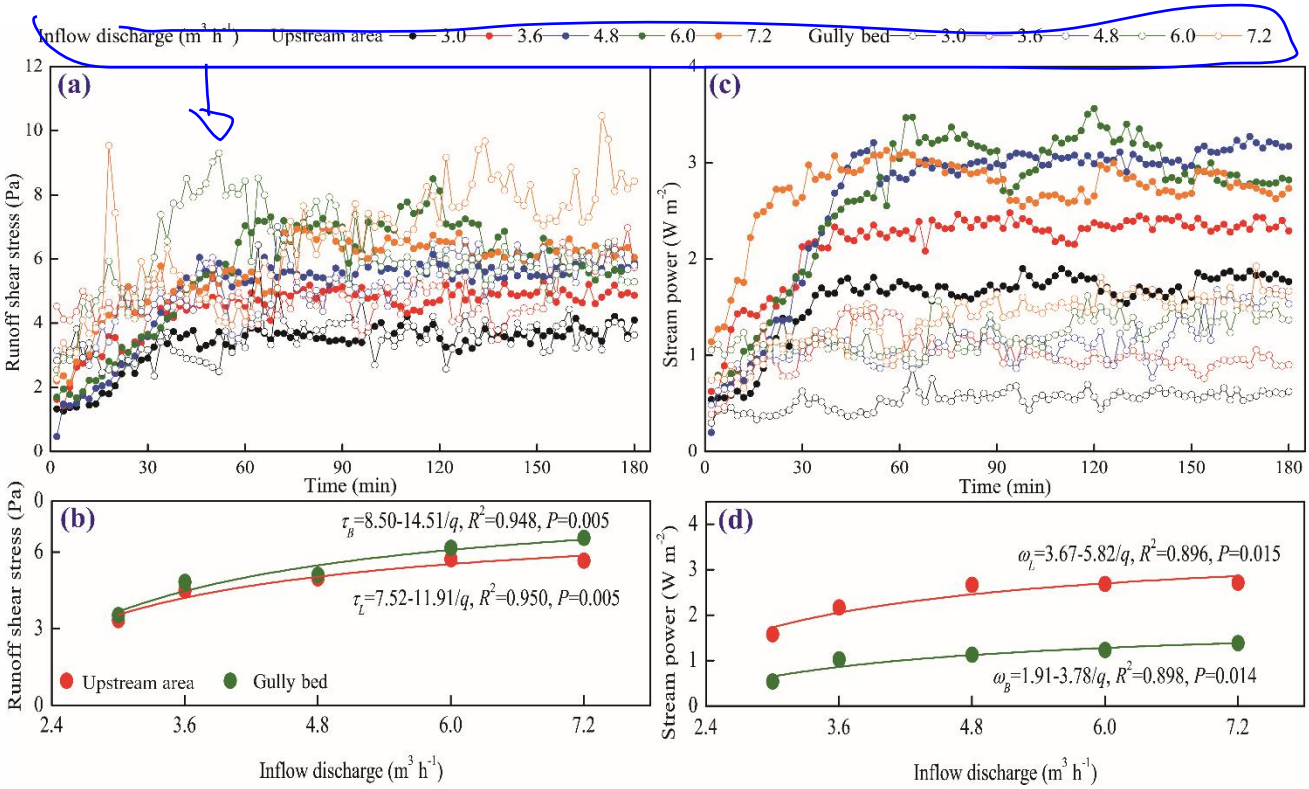

Fig.8 Temporal changes in runoff shear stress and stream power of upstream area and gully bed and their relationships with inflow discharge

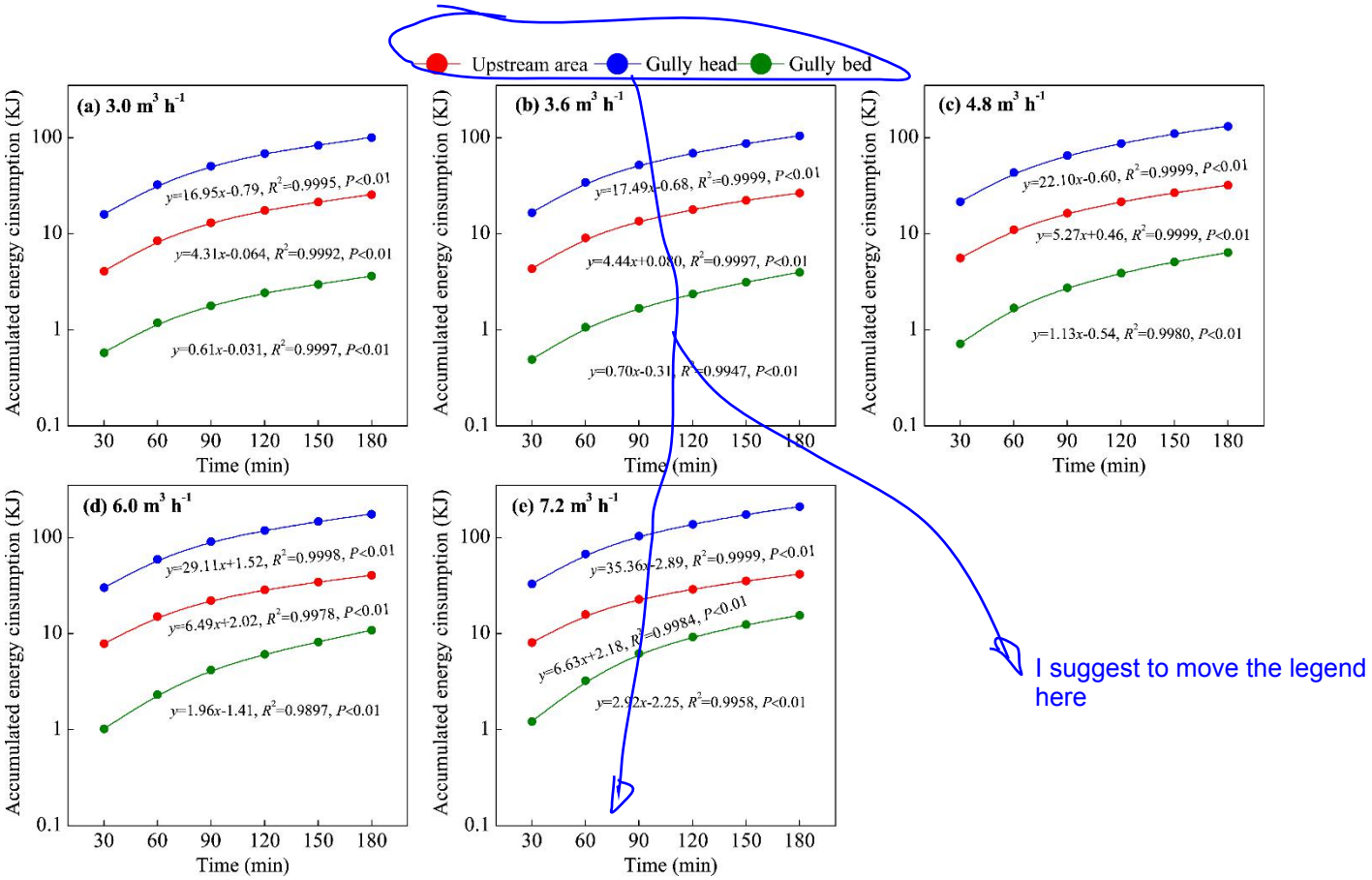

Fig.9 Temporal changes in runoff energy consumption of upstream area, gully head and gully bed under different inflow discharge conditions

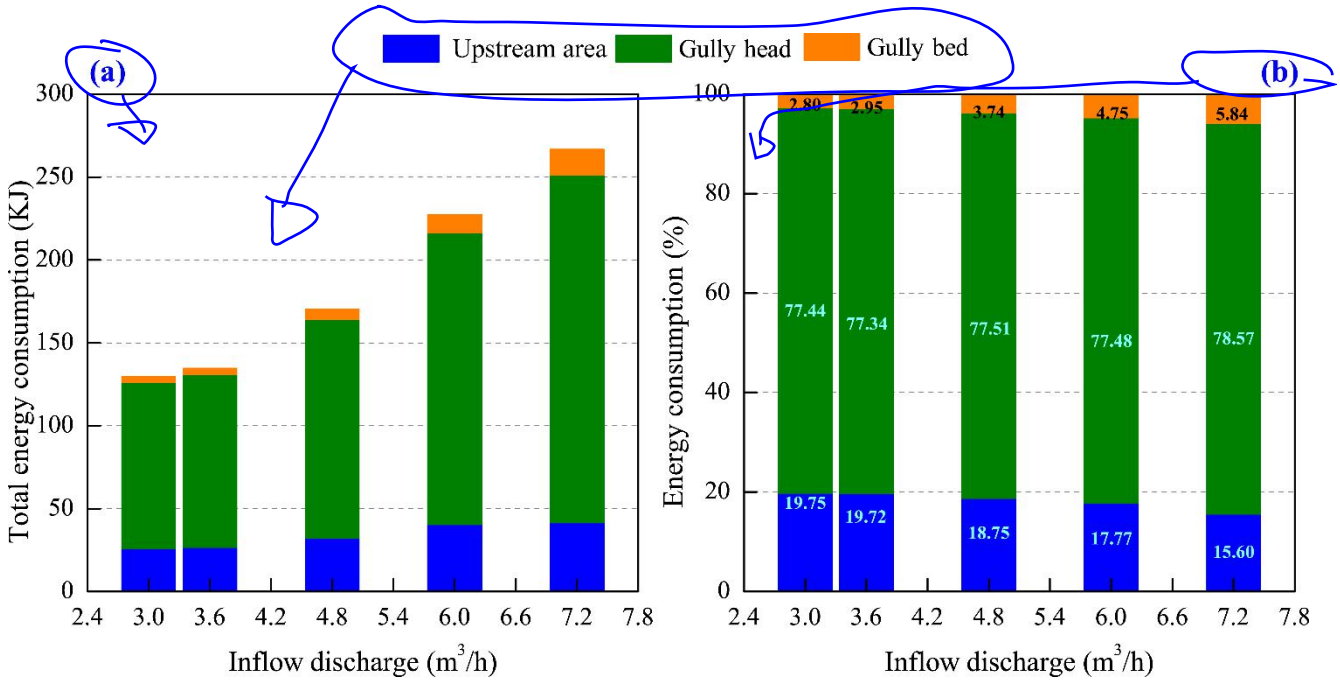

Fig.10 The variation in energy consumption of upstream area, gully head and gully bed and their proportions with inflow discharge

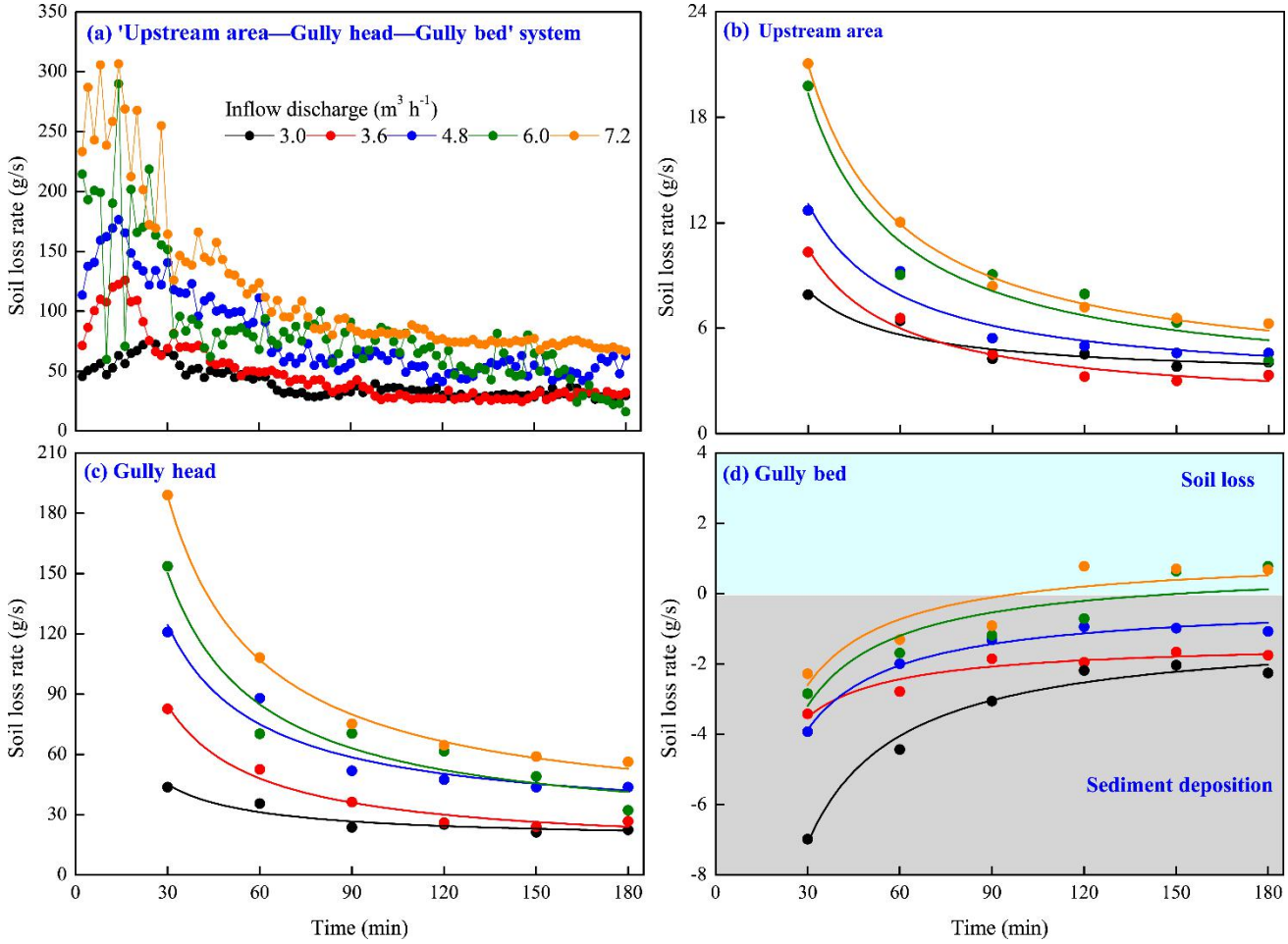

884

885 Fig. 11 Temporal variation in soil loss rate of the “upstream area—gully head—gully bed” system and each

886 landform unit

887

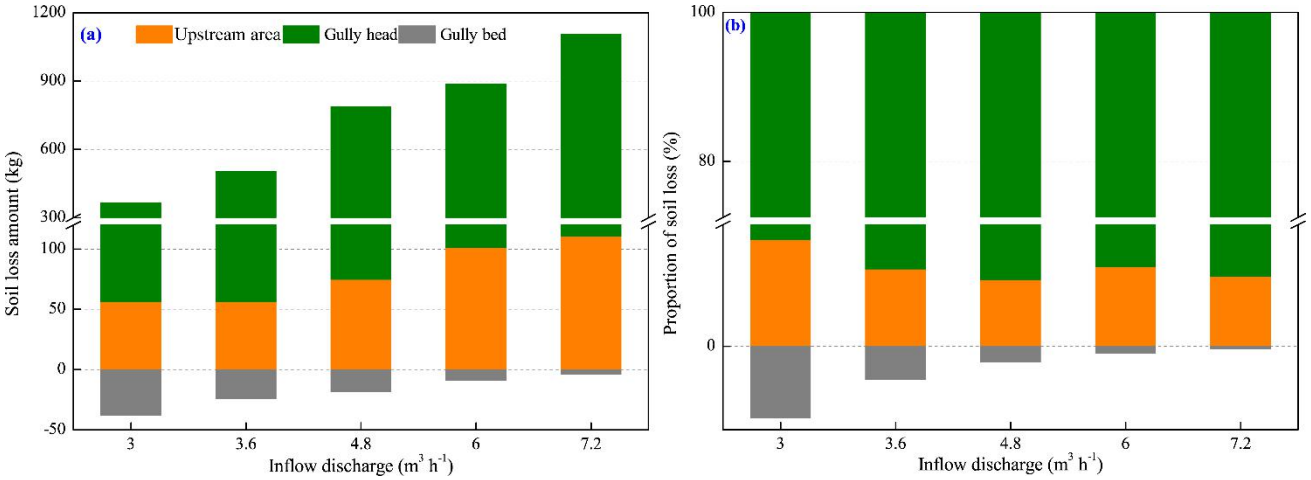

888

889 Fig. 12 Variation in soil loss amount and proportion of upstream area, gully head and gully bed with inflow

890 discharge

891

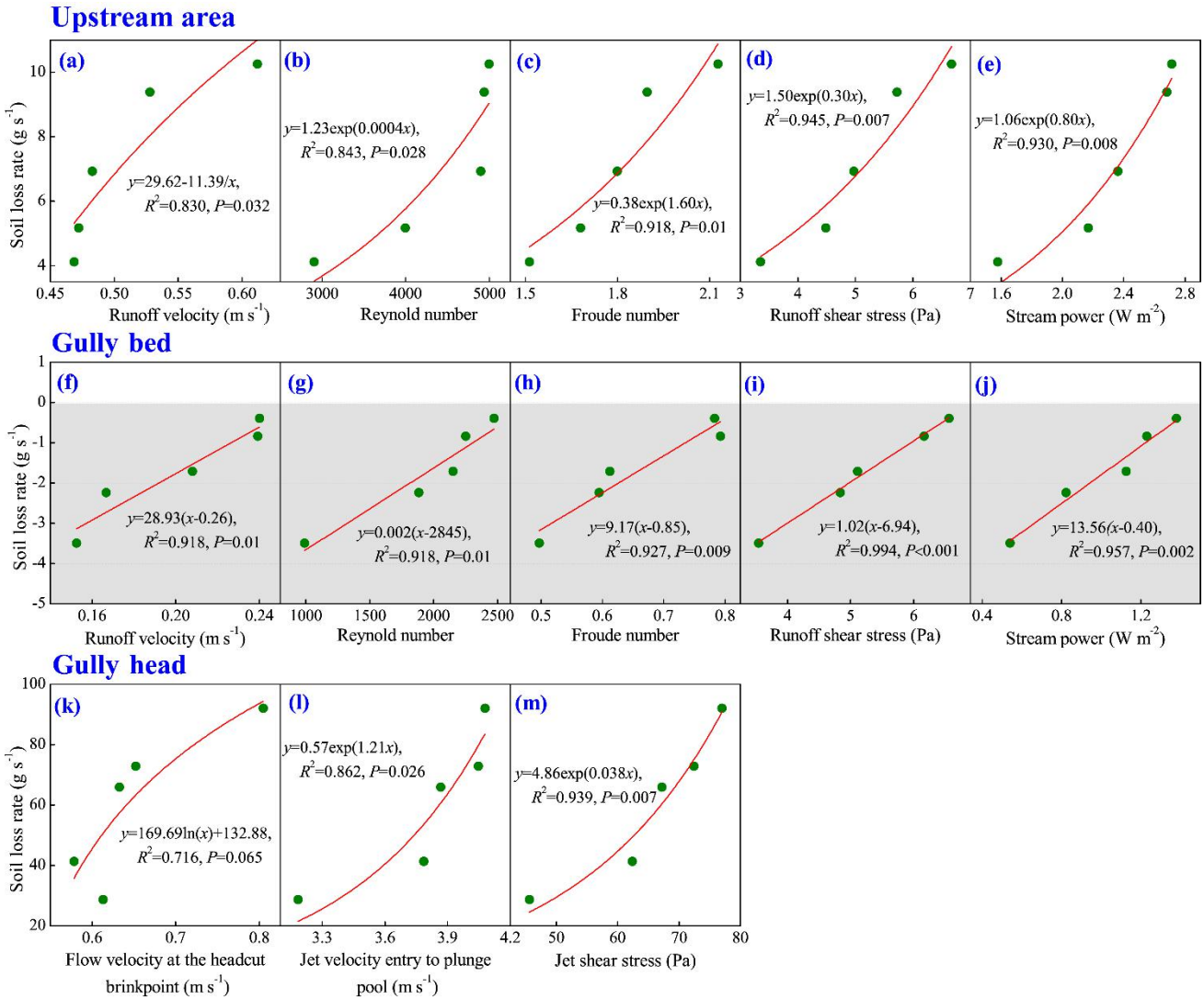

892

893 Fig. 13 Relationships between soil loss rate of three landform units and hydraulic and jet properties

894

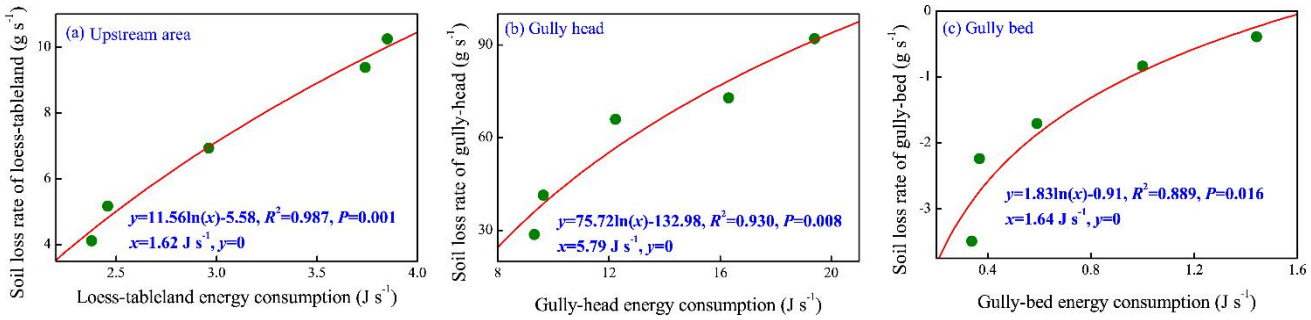

Fig. 14 Relationships between soil loss rate of three landform units and runoff energy consumption